Self-consistent calculations of the electric charge, ion drag force, and the drift velocity of spherical grains using Langevin Dynamics and comparisons against canonical experiments

Venkata Madugula[†], Vikram Suresh[†$], Zhibo Liu[†], Davis Ballard[†], Logan Wymore[#], and Ranganathan Gopalakrishnan[†*]

[†]Department of Mechanical Engineering, The University of Memphis, Memphis, TN 38152

[#]Arlington High School, Arlington, TN 38002

Submitted for peer review to *Physics of Plasmas*

*Corresponding author email: rgplkrsh@memphis.edu

[$]Current address: Micron Technology Inc., Boise, ID 83716

Abstract

We present trajectory simulation-based modeling to capture the interactions between ions and charged grains in dusty or complex plasmas. Our study is motivated by the need for a self-consistent and experimentally validated approach for accurately calculating the ion drag force and grain charge that determine grain collective behavior in plasmas. We implement Langevin Dynamics in a computationally efficient predictor-corrector approach to capture multiscale ion and grain dynamics. Predictions of grain velocity, grain charge, and ion drag force are compared with prior measurements to assess our approach. The comparisons reveal excellent agreement to within $\pm 20\%$ between predicted and measured grain velocities (*Phys. Plasmas* **12**(9): 093503 and *Europhysics Lett.* **97**: 35001) for $0.64, 1.25\ \mu m$ grains at $\sim 20 - 500\ Pa$. Comparisons with the measured grain charge (*Phys. Rev. E* **72**(1): 016406) under similar conditions reveal agreement to within $\sim 20\%$ as well. Measurements of the ion drag force (*Phys. Plasmas* **11**(12): 5690 and *IEEE Trans. Plasma Sci.* **32**(2): 582) are used to assess the viability of the presented approach to calculate the ion drag force experienced by grains exposed to ion beams of well-defined energy. Excellent agreement between calculations and measurements is obtained for beam energies >10 eV and the overprediction below 10 eV is attributed to the neglect of charge exchange collisions in our modeling. Along with critical assessments of our approach, suggestions for future experimental design to probe charging of and momentum transfer onto grains that capture the effect of space charge concentration and external fields are outlined.

1. Introduction

The relative motion of ions with respect to objects/grains in a plasma leads to the ion drag force [1-5], like the drag force experienced by surfaces immersed in flows of neutral fluids. Ion drag force $\vec{F}_{id}$ plays a critical role in the collective motion and self-organization of grains in plasmas [6, 7], void formation in complex plasmas [8-11] as well as in ionic propulsion systems, coronal mass ejections, spacecraft dynamics in the ionosphere. Specifically, laboratory complex plasma experiments containing deliberately introduced well-characterized spherical microparticles amenable for optical tracking have been used to experimentally probe the ion drag force [12-22] on individual grains owing to ion streaming driven by electric or magnetic fields or directed kinetic energy in beams. These experimental studies have unraveled the nature of the ion drag force on spherical grains and provide data for evaluating the predictions of modeling approaches.

The ion drag force $\vec{F}_{id}$ is the combined effect of the long-range electrostatic interactions between ions and grains (called orbit force $\vec{F}_o$) and the momentum transferred onto the grain by the ion upon impact (called collection force $\vec{F}_c$): $\vec{F}_{id} = \vec{F}_o + \vec{F}_c$. The orbit force $\vec{F}_o$ is influenced by the electrostatic potential energy of the ion $z_i e\varphi_p$, where z_i is ion elementary charge and φ_p is the electrostatic potential field in which the ion moves, ion thermal energy $k_B T_i$ (T_i is the ion temperature), and the electric field $\vec{E}_o$ and/or magnetic field $\vec{B}_o$ causing the ion drift or the directed mean kinetic energy of the ion U_o if produced as a beam. The collection force $\vec{F}_c$ is a consequence of the transfer of the packet of momentum $m_i\vec{v}_i$ carried by the ion on to the grain upon impact and subsequent recombination through an electron transfer from the grain surface. Several non-linear feedback loops determine φ_p and render the modeling of ion drag a fascinating and challenging endeavor:

- The grain charge z_p, that plays a dominant role in setting φ_p, is established by the competition between ion current I_i and electron current I_e to the grain as well as surface electron emission processes [23]. The space charge in the plasma (electrons, ions, and grains) also determine φ_p through the Poisson equation.
- The extent to which φ_p is anisotropic is determined by the ion Mach number $M_T = \frac{v_{id}}{v_T}$ to quantify the relative importance of the collective ion flow or drift speed v_{id} compared to ion thermal speed v_T with φ_p being perfectly isotropic in the limit of $M_T \to 0$ and the extent of distortion increasing with M_T.
- φ_p distortion is negligible in the limit of $\frac{\lambda_{ii}}{a_p} \to \infty$ and significant enough to influence ion transport otherwise, where a_p is the grain size (radius) and λ_{ii} is the ion mean free path with respect to ion-ion scattering.
- The spatial distribution of ions around the grain also influences φ_p. Due to scattering of the momentum of drifting ions due to collisions with neutral gas molecules as a

function of the gas pressure p_g, directed ion kinetic energy is randomized into thermal energy that increases ion capture by the grain as well as influences momentum transfer to the grain. In the limit of $\frac{\lambda_{in}}{a_p} \to \infty$ ($p_g \to 0$), ion motion is collisionless with respect to neutrals and in the opposite limit $\frac{\lambda_{in}}{a_p} \ll 1$ ($p_g \to \infty$), ion trajectories are diffuse due to Brownian motion; λ_{in} is the ion-neutral mean free path.

$\vec{F}_{id}$ depends on grain size and shape, plasma discharge parameters (electron temperature T_e, ion temperature T_i, plasma ion, electron number density n_e and neutral gas pressure p_g, temperature T_g), and combinations of $\vec{E}_o, \vec{B}_o, U_o$ driving ion flow. A long-standing modeling question is to provide a comprehensive description of the ion drag force $\vec{F}_{id}$ for various ion flow regimes and validate the same against available experimental data as well as motivate future experimental design. In this article, we describe Langevin Dynamics (LD) based trajectory simulations of a spherical grain interacting with an ion flow consistent with the experimental datasets chosen for validation. We defer the consideration of the grain shape effect to potential future investigations. Consistent with the plasmas formed in rare gases ($Ar, Ne, He, \ldots$) in the cited complex plasma experiments, we model our ions as singly charged positive ions ($Ar^+, Ne^+, He^+, \ldots$). Multiply charged molecular ions or those derived by the ionization of electronegative gases [24] may be considered using the presented computational approach, although we refrain from doing so within this article. We also choose to exclude magnetized ions flows [25, 26] in the present work and assume $\vec{B}_o = 0$. Finally, the loss (recombination) and production (ionization) of plasma, and resonant charge transfer between ions and neutrals [27-29] also affects the ion drag force [30] and such contributions can also be included in the current approach in the future. The validation of the computational methodology against experimental data demonstrated in this work sets the stage to revisit the simplifications made here using the described approach. Lastly, analogous to the ion drag force, grains subject to electron flows experience an electron drag force as well. Due to much lesser mass of electrons than ions or neutrals and their higher temperatures in gas discharges used for complex plasma experiments ($k_B T_e \sim 1 - 10\ eV, k_B T_i \sim 0.03\ eV$), their contribution to the grain force balance can be neglected without much consequence when $\frac{T_e}{T_i} > 33$ and $E_0 < 300 \frac{V}{m}$ [31]. In the absence of significant electron temperature gradient (conditions where a single value of T_e accurately denotes the electron population), the electron thermal force may also be ignored. For the experimental conditions chosen for validation, the electron drag force is unlikely to contribute significantly and we do not consider electron-induced thermal and drag forces further. We present the need and objectives of this modeling effort by reviewing the current state of the art in modeling ion drag force.

2. State of the art

In the collisionless limit of $\frac{\lambda_{ii}}{a_p} \to \infty$ and $\frac{\lambda_{in}}{a_p} \to \infty$, scattering of positive ions by a negatively charged grain has been analyzed using classical Coulomb and Yukawa scattering approaches, reviewed in detail elsewhere [3, 32]. A binary collision formalism is applied to derive the Orbital Motion-limited model for the ion flux, ion momentum flux, and ion thermal energy flux to spherical grains. Specifically, the momentum transfer cross-section $\sigma(\vec{v}_i, b)$ is derived by applying angular momentum and energy balance for a single ion-grain pair where $\vec{v}_i$ is the ion velocity and b is the impact parameter of the collision. The ion drag force $\vec{F}_{id} = \int \vec{v}_i \, v_i \sigma(\vec{v}_i, b) f_i(\vec{v}_i) d\Omega_{\vec{v}_i}$ where $f_i(\vec{v}_i)$ is the ion velocity distribution function, v_i is the ion speed and $d\Omega_{\vec{v}_i}$ is the differential volume element in the velocity phase space over which integration is carried out. Various approximations have been proposed for $\sigma(\vec{v}_i, b)$ for different forms of the interaction potential φ_p driving ion trajectories [33-46].

The binary collision approach has been used to derive semi-analytical expressions for $\vec{F}_{id}$ for sub-thermal ($M_T \ll 1$) and suprathermal ($M_T \gg 1$) ion flows [47]. A viable model for the transonic ion flow regime $M_T \sim 1$ is yet to be developed even for collisionless conditions (low pressure and/or small grains). This regime marks the transition between thermally driven ion motion and super-sonic motion leading to the formation of ion-acoustic waves. Further, the classical coulomb scattering approach does not consider ion-neutral collisions. This is a major drawback in using this approach for tackling ion flows in finite pressure plasmas [1]. One of the remedies proposed to account for ion-neutral collisions is to employ a self-consistent kinetic theory approach in which the Boltzmann equation for ion velocity distribution function $f_i(\vec{v}_i)$ is solved for with the Bhatnagar-Gross-Krook (BGK) approximation for the ion-neutral collision operator. The grain-ion potential φ_p is coupled to the Boltzmann equation through the Poisson equation. The ion-neutral collisions are modeled to be of constant (fixed) frequency to derive an integral expression for ion drag that depends on the plasma response to the ion flow and gas pressure as well [48, 49]. The kinetic approach provides simple analytical asymptotes for $\vec{F}_{id}$ in the $M_T \ll 1$ and $M_T \gg 1$ ion flow regimes while numerical methods may be employed in the intermediate M_T regime [50-52]. The kinetic approach [53, 54], while rectifying some of the deficiencies of the binary collision approach, does not provide any information about ion trajectories and spatial distribution around the grain which has motivated the development of trajectory simulations that provide fine details of ion motion and allow the self-consistent inclusion of various interactions. Trajectory simulations are capable of simultaneously predicting the grain charge and ion drag force amenable for direct comparison with canonical experiments. To avoid a direct numerical simulation of electron, ion, and grain motion which span several orders of magnitude in characteristic timescales and requires computational resources that are practically not possible with

even the most powerful computers of the day, various approximations have been used within the framework of trajectory simulations which we summarize next before crystallizing the objectives of the current modeling effort.

The SCEPTIC code [55-57] has been used to compute the ion drag force on a spherical grain [58] as a function of the ion drift velocity in the collisionless limit $\left(\frac{\lambda_{in}}{a_p} \to \infty, p_g \to 0\right)$. In this formalism, ion motion in the electrostatic potential field φ_p is tracked explicitly to evaluate $\vec{F}_{id}$ including ion collection and orbital motion contributions. In that process, the ion current collected by the grain is also self-consistently obtained. The free electron number density near the grain n_e is calculated as $n_{e\infty}e^{\frac{e\varphi_p}{k_B T_e}}$ where the Boltzmann factor $e^{\frac{e\varphi_p}{k_B T_e}}$ accounts for electron depletion due to the presence of the grain itself. φ_p is updated after each timestep by solving the Poisson equation to account for the varying space charge environment around the grain. A field representation of the ion number density n_i is calculated as the average number of ions per grid volume. Later, ion-neutral collisions were included using a Monte Carlo approach (also called null collision method [59]) wherein at each timestep, a uniform random number is used to decide whether an ion suffer a scattering collision with a neutral molecule or not to calculate the collisional ion current to a grain [60] and ion drag force at finite gas pressures [61]. While this approach captures the effect of ion-neutral collisions at low pressures well, it fails to include the systematic drag force experienced by ions due to their relative motion with respect to the gas. Nevertheless, the SCEPTIC code (for a single grain) and the COPTIC code (for multiple grains) have been used for investigating charge and momentum transfer onto grains in flowing plasmas and for understanding the structure of ion wakes formed downstream of grains [62, 63]. Our approach in this article is inspired by the pioneering approach took by Hutchinson and co-workers through a series of articles to investigate the ion drag force in instances of combined electric and magnetic fields [64, 65], grain-grain interactions in supersonic ion flows [66], and collisional effects on such forces [67, 68]. Also using a PIC approach, Ikkurthi, Matyash, Melzer and Schneider [69] have carried out calculations of charge and ion drag on a static spherical grain using the P3M code and have used the Monte Carlo approach for including ion-neutral collisions and later extended the approach for small clusters of grains [70]. More recently, Sundar and Moldabekov [71] have considered the flow non-Maxwellian ions past two grains to study ion wake formation while including the fully coupled solution of the Poisson equation to obtain the potential profile around the grains instead of relying on linear superposition.

Piel [72] developed the MAD code in which superparticles are used to represent the ion population and are tracked explicitly in the electrostatic potential field φ_p. The superparticles (we call them superions for clarity) are point charges with the same charge to mass ratio as the ions and are assumed to represent a certain of ions to reduce the number of operations and computational resources required for the simulation. The

analytical form of φ_p is derived by considering approximations for n_e in the Poisson's equation under various regimes of the ratio of $|e\varphi_p|$ and $k_B T_e$. Like SCEPTIC, the free electron number density near the grain n_e is calculated as $n_{e\infty} e^{\frac{e\varphi_p}{k_B T_e}}$ using the Boltzmann factor $e^{\frac{e\varphi_p}{k_B T_e}}$. In the limit of $|e\varphi_p| \gg k_B T_e$, $n_e \cong 0$ and φ_p is determined entirely by grain-superion bare Coulombic interactions without shielding. For $|e\varphi_p| \ll k_B T_e$, the Poisson equation is linearized and φ_p is shown to be the sum of the contributions of the superions interacting with the grain through a shielded Coulomb potential with an effective Debye length $\lambda_{D_e} = \sqrt{\frac{\varepsilon_0 k_B T_e}{n_{e\infty}}}$. For intermediate $\frac{|e\varphi_p|}{k_B T_e}$ combinations, grain-superion interactions are taken to be bare Coulombic potential while superion-superion interactions are modeled as shielded Coulombic potential. While the superions are a construct, calculations of the ion drag and ion wake structure using MAD agree well with the SCEPTIC code-derived results. Notably, the MAD code is designed to simulate collisionless ion flows and can be used to investigate the interaction of superions with a single grain or multiple grains. Piel and co-workers have used MAD to study forces on grains in magnetized plasma flows [73-77].

More recently, Matthews, Sanford, Kostadinova, Ashrafi, Guay and Hyde [78] have developed the DRIAD code which treats superion-grain interactions exactly as in the MAD code [72]. Importantly, the superion concept is retained. To accurately resolve both the ion and grain timescales (μs vs. ms), DRIAD tracks the superions for ~100-200 timesteps chosen to resolve superion motion, and then the simulation switches to the grain scale while the ions remain frozen. Using a timestep based on the grain timescale, where the grain motion is advanced for one timestep and the simulation switches back to the ion scale. The change in grain charge ΔZ_p in each timestep (in the superion scale) is calculated as the sum of the number of ions ζ_i and the number of electrons ζ_e that cross the grain surface: $\Delta Z_p = q_s \zeta_i - \zeta_e$; q_s is the charge number of a superion. ζ_i is obtained directly from the trajectory calculations. ζ_e is estimated as $I_e^{OML} \Delta t_i$ where Δt_i is the superion-scale timestep. The superion and grain scales are iteratively simulated until the average values of the ion number density in the domain and grain charge stabilize to a steady state. The DRIAD method speeds up the convergence of both the grain and ion velocities due to the multi-scale iteration. DRIAD has been used to the ion wake structure, confinement and interaction forces between grains and has reproduced features seen in experiments as well [79].

When taken together, the SCEPTIC, MAD, and DRIAD trajectory simulation codes offer useful insights for developing a robust approach for self-consistently simulating the interaction between an ion flow and grain(s) while including pertinent potential interactions and the effect of neutral gas that we summarize in **Table 1**. In this article, we describe a Langevin Dynamics-based trajectory simulation approach to simulate complex plasmas that can potentially overcome the conceptual and computational limitations of these

pioneering approaches to calculate the ion drag force on a spherical grain. We also recognize that since ion transport to a grain contributes to the collection force, the grain charge needs to be calculated self-consistently from any trajectory simulation simultaneously accounting for the ion and electron currents [2, 32, 80] to the grain. The modeling of ion current to a *stationary* grain with *fixed* charge immersed in an isotropic (stationary) plasma has a long and rich history [60, 81-105]. In the presented approach, the grain charge, grain drift velocity and ion drag force experienced by the grain are calculated until convergence is attained towards a steady state. By tracking the trajectories of individual ions, our approach self-consistently includes fluctuations in the electric charge [106, 107] due to the discrete number of ions and electrons collected by the grain and its effect on the ion drag force and grain velocity starting with only the plasma conditions as input. Detailed comparisons of the predictions of observables (grain drift velocity, ion drag force, grain charge) against pertinent experimental data are presented to provide a comprehensive validation of our approach. A summary of prior ion drag and charging experiments listed in **Table 2** follows next.

Prior complex plasma experiments recorded the trajectories of spherical grains and subsequently used the position and velocity data to infer the ion drag force and/or grain charge. Zafiu, Melzer and Piel [12] conducted the first demonstration that the total force on grains in a plasma is made up of the ion drag force, electric force, and thermophoretic force. In a follow up study, Zafiu, Melzer and Piel [13] measured the ratio of the ion drag force to electric force for various grain diameters and neutral gas pressures. In their experiments, ion drag force was seen to be stronger than the electric force thus making it likely to drive grain motion in complex plasmas. They measured the deflection of the trajectory of free-falling microspheres through a variable electric field along with detailed characterization of the plasma potential profile and temperature profile to accurately estimate the grain forces for comparisons with models. The experiments of Zafiu, Melzer and Piel [13] spurred discussion [108, 109] on the choice of plasma screening length based on the electron Debye length and also about the complexity in determining the ion drag force both experimentally and computationally. Following a similar approach, Hirt, Block and Piel [15] measured the deflection angle of the grain trajectories in free fall to infer the ion drag force directly. They also showed that in their experimental setup, thermophoretic force did not contribute to grain deflection. So, their measurements directly yielded the drag force as a function of the ion beam energy $U_0 \sim 3 - 45\ eV$ at low pressure ($\sim 10^{-2} - 10^{-1}\ Pa$) and in a follow-up study [14] at high pressure ($\sim 7.2\ Pa$). Later, Nosenko, Fisher, Merlino, Khrapak, Morfill and Avinash [18] carried out accurate measurements of the ion drag force with detailed characterization of the discharge conditions and provided excellent data for model validation at ion concentrations ~ 100 times higher than that of Hirt, Block and Piel [14] and Hirt, Block and Piel [15]. For our purposes, we use data from Hirt, Block and Piel [15] and Hirt, Block and Piel [14] to test

if our approach can calculate the ion drag force due to an ion beam of known energy and number density but without an electric field driving the ions.

Apart from these ground-based experiments, the Plasma Krystal-4 (PK4) experiment on board the International Space Station has been used in several studies to record grain trajectories in response to a DC electric field under known discharge conditions [110-115]. In these experiments, grain trajectories (position and velocity timeseries for each grain in the camera frame) are the raw data used to calculate the steady state drift velocity of the grains [20]. By applying a force balance on a nominally isolated grain interacting with ions, electrons, and neutrals, the ion drag force has been estimated [16, 17]. Alternately, by treating the ion drag force using a suitable model, the force balance on a single grain has also been solved to obtain the grain charge as well [22, 116-118]. As we describe later, our trajectory simulation approach yields the ion drag force, electric force or charge, and the neutral drag force or grain drift velocity simultaneously. We compare our calculations against the raw data (time-averaged grain drift velocity) wherever available. In other instances, we compare our predictions with the reported ion drag force or grain charge.

The rest of the article is organized as follows: The Langevin Dynamics (LD) trajectory simulation approach is described in the *Methods* section. Following that, we present comparisons of simulation predictions with noted experimental data along with detailed discussion of our findings in *Results and Discussion*. Finally, we summarize our *Conclusions* along with suggestions for improvements and future investigations.

3. Methods

The complex plasma formed in an inert gas consists of four components: positive ions, electrons, neutral gas molecules or neutrals, and $\sim nm - \mu m$-sized grains. As such, a direct numerical simulation of the trajectories of these four components is unfeasible due to the enormous number of simultaneous equations of motion that need to be integrated and the disparity in the timescales of their motion. As has been done in prior trajectory simulation approaches [55, 72, 78], we use a combination of approximations for each species to develop a computationally tractable approach. Our goal is to accurately resolve the trajectory of a grain while accounting for the effect of ions, electrons, and neutrals on the same and elicit predictions that can be directly compared with a complex plasma experiment in a time-averaged sense.

For plasmas containing hot electrons $(k_B T_e \sim 1 - 10\ eV)$ and room-temperature ions $(k_B T_i \sim 0.03\ eV)$ that are in thermal equilibrium with the neutrals at low to moderate pressures $(p_g < 1000\ Pa)$, the electron is implicitly represented and justified as follows: The potential energy of interaction of the electrons with grains, ions, and with each other is much smaller than their thermal energy. Consequently, we assume a free electron gas model with a mean temperature T_e. For electric field $E_0 < \sim 300 \frac{V}{m}$ and for electron to ion

temperature ratio $\tau = \frac{T_e}{T_i} > 33$, both of which are true for the datasets chosen here for validation (**Table 2**), electrons do not respond to any grain, ion forces or electric fields in the system and need not be tracked explicitly in simulations. To evaluate this assumption, we conducted trajectory simulations with electrons of temperature $T_e = 1\ eV$ in an applied field $E_0 = 200\frac{V}{m}$, that is a typical value in the validation datasets, interacting with a single spherical grain. Figure S1 in Section S1, Supplemental Material (*SI*), displays the electron velocity distribution function for $E_0 = 0$ and $E_0 = 200\ \frac{V}{m}$. It is clearly seen that the electron velocities are not modified due to electron-electron Coulombic forces and the applied electric field. Further, electron motion is collisionless with respect to the neutrals and the electron flux coefficient β_e is routinely calculated using the orbital motion-limited theory [91, 92] that depends on the grain-electron potential energy $-e\varphi_p$ and electron thermal energy $k_B T_e$ (m_e is electron mass):

$$\beta_e = \left(\frac{8k_B T_e}{\pi m_e}\right)^{\frac{1}{2}} \pi a_p^2 \begin{cases} \exp\left(\frac{e\varphi_p}{k_B T_e}\right), \varphi_p \leq 0 \\ 1 + \frac{e\varphi_p}{k_B T_e}, \varphi_p > 0 \end{cases} \quad \dots (1)$$

β_e calculated using eq. 1 $\left(8.2 \times 10^{-5}\frac{m^3}{s}\right)$ agrees reasonably well the collisionless simulation with $E_0 = 0$ $\left(7.65\ \times 10^{-5}\frac{m^3}{s}\right)$. Further, β_e with $E_0 = 200\frac{V}{m}$ is $7.78 \times 10^{-5}\frac{m^3}{s}$. From these calculations, we infer that the effect of electron concentration n_e is weak at $n_e{\sim}10^{14}\ m^{-3}, T_e{\sim}1\ eV$ and the effect of electric field is insignificant and is neglected for $E_0 \leq {\sim}200\frac{V}{m}$. Due to grain concentration $n_p \ll n_e$, we assume that the electron current to the grain does not significantly deplete the plasma electron density which we consider to be spatially homogeneous. This allows us to use eq. 1 to estimate electron current $I_e = \beta_e n_e$ to a grain assuming the dependencies of β_e on n_e, E_0 may be ignored for the present purposes. We note that future modeling would need to parameterize the effects of electron-electron interactions (n_e) and plasma anisotropy (E_0) on β_e.

The MAD and DRIAD codes that track superions, consider the screening of superion-superion interaction due to electrons. In our simulation, the average force on ions due to electrons is taken to be zero assuming that the electrons are uniformly distributed around individual ions. Hence, we use a bare Coulomb interaction for ion-ion interactions. Similarly, the electron density near a negatively charged grain is reduced due to absorption of high-energy electrons by the grain and the repulsion of low-energy electrons. Consequently, we also consider the force on grains due to electrons is also nominally negligible and use bare Coulombic interactions for both grain-ion and grain-grain electrostatic forces. We reiterate that this assumption is valid for electric field strengths $E_0 < {\sim}300\frac{V}{m}$ and for hot electrons considered here with $\frac{T_e}{T_i} > {\sim}33$. In these

conditions, the electric field, and the presence of other charges notwithstanding, electron motion is isotropic as confirmed by our collisionless trajectory simulation of electrons.

It is of interest to track ion and grain trajectories *explicitly* while accounting for electrostatic forces. The effect of neutrals on ion and grain motion is *implicitly* accounted here using a Langevin model [119-124] wherein the short timescale fluctuations in ion/grain momentum are captured by adding a stochastic Brownian force $\vec{F}_B$ and the long timescale drag exerted by the relative flow of neutrals past the ion/grain is accounted through the neutral drag force $-f\vec{v}$; f is the ion/grain friction factor or momentum loss coefficient (with units of $\frac{kg}{s}$) and $\vec{v}$ is ion/grain velocity with respect to the neutral gas. $\vec{F}_B$ is a normally (Gaussian) distributed random vector used to model the ion/grain-neutral scattering events with the following statistical properties: $\int_0^{t_r} \vec{F}_B(t')dt' = 0$ and $\int_0^{t_r} \vec{F}_B(t_r) \cdot \vec{F}_B(t'-t_r)dt' = 6fk_BT_g\delta(t_r)$, where t_r is an arbitrary interval of time much longer than the ion/grain momentum relaxation time $\sim\frac{m}{f}$ $\left(t_r \gg \frac{m}{f}\right)$; m is the mass of ion/grain. We simulate the motion of ions and a single grain without having to explicitly track the neutrals using Langevin Dynamics (LD). In prior work, we have used LD simulations to develop experimentally validated models of grain charging in aerosols [86, 125-129] and isotropic or stationary dusty plasmas [85].

The simulation domain is a periodic box of volume L^3 that represents an infinitesimal volume in real space wherein the ion concentration n_i is uniform. N_i ions are used to attain desired $n_i = \frac{N_i}{L^3}$. Our approach is to simulate a nominally isolated grain interacting with a population of ions in general $\left(n_p^{-\frac{1}{3}} \gg n_i^{-\frac{1}{3}}\right)$, for which we present calculations and validations; n_p is dust concentration. An electric field $\vec{E}_0 = E_0\hat{\imath}$ acts on the ions and grain. The timescale of ion motion t_{ion} is smaller than that of the grain t_p by ~ 4 orders of magnitude and presents a computational challenge. Using a small enough timestep to resolve ion motion leads to very slow convergence of the grain phase dynamics and use of a timestep on the scale of grain motion leads to large sampling errors for the ion trajectories. Inspired by the DRIAD code, we use a multiscale predictor-corrector approach summarized in **Figure 1**.

In the ion scale *predictor* step, the grain (of radius a_p, density ρ_p, and mass $m_p = \rho_p \frac{4\pi}{3} a_p^3$) is placed at the center of the domain and is held stationary. N_i ions (each of mass m_{ion} and charge $z_{ion} = +1$) are tracked explicitly by integrating Langevin equations of motion using a first-order time-stepping scheme [130]:

$$m_{ion}\frac{d\vec{v}_i}{dt} = -f_{ion}\vec{v}_i + \vec{F}_i^B - \sum_{j=1,j\neq i}^{N_i} \nabla\frac{z_{ion}^2 e^2}{4\pi\varepsilon_0 r_{ij}} - \nabla\frac{z_{ion}z_p(t)e^2}{4\pi\varepsilon_0 r_{ip}} - z_{ion}e\nabla E_0\left(r_{ip} - \frac{a_p^2}{r_{ip}}\right)\cos\theta_{ip} \ldots (2)$$

$f_{ion} = \frac{|z_{ion}|e}{\mu_{ion}}$ is the ion friction factor calculated using ion mobility μ_{ion} as described in Section S2, *SI*. $r_{ij} = |\vec{r}_j - \vec{r}_i|$ is the distance between entity i with position vector $\vec{r}_i$ and entity j with position vector $\vec{r}_j$ and θ_{ij} is the polar angle between $\vec{r}_i$ and $\vec{r}_j$ in an axial coordinate system aligned with the x-axis; p refers to the grain. $-z_{ion}e\nabla E_0\left(r_{ip} - \frac{a_p^2}{r_{ip}}\right)\cos\theta_{ip}$ is the force on ion i due to the electric field that considers the field distortion due to the grain. $-\sum_{j=1,j\neq i}^{N_i}\nabla\frac{z_{ion}^2e^2}{4\pi\varepsilon_0 r_{ij}}$ and $-\nabla\frac{z_{ion}z_p(t)e^2}{4\pi\varepsilon_0 r_{ip}}$ are the pairwise Coulombic forces due to other ions and grain of instantaneous charge $z_k(t)$, respectively, on ion i. The grain, while stationary, receive ion and electron fluxes that affect the instantaneous charge $z_p(t)$ updated after each timestep, with $z_p(t=0) = 0$:

$$z_p(t + \Delta t) = z_p(t) + \zeta_i - \zeta_e \ldots (3a)$$

ζ_i is the number of ions that cross over into the grain $(r_{ip} \leq 1)$ in a single timestep Δt_i, ζ_e is the number of electrons transported onto the grain. Electron current flow to the grain is much faster than ion transport and ζ_e is estimated as a random number sampled from a Poisson distribution with mean parameter $\Lambda_e = \frac{I_e}{e}\Delta t_i$, where I_e is given by eq. 1 and Δt_i is the simulation timestep. We note that while DRIAD adds Λ_e (non-integer) electrons at each timestep while we adopt a Monte Carlo approach to model the collection of an integer number of electrons more accurately by a grain over a time interval Δt_i. DRIAD also considers only $\vec{F}_i^B$ in the ion force balance and does not account for the systematic resistance to ion motion due to neutral drag on the same. After the ion velocity distribution stabilizes, at each subsequent timestep the force on the grain due to all N_i ions is computed:

$$\vec{F}_p(t) = -\sum_{i=1}^{N_i}\nabla\frac{z_{ion}z_p e^2}{4\pi\varepsilon_0 r_{ip}} \ldots (3b)$$

After $N_t \sim 50 - 200$ grain-ion collision events (after stabilization of the ion velocity distribution function), the simulation switches to the grain scale corrector step wherein the ions are not simulated directly – the time-averaged force $\langle\vec{F}_p\rangle_t$ exerted by the ions on the grain is included in eq. 5 to capture the effect of the ions on grain motion:

$$\langle\vec{F}_p\rangle_t = \frac{\sum_{l=1}^{N_t}\vec{F}_p(t)\Delta t_l}{\sum_{l=1}^{N_t}\Delta t_l} \ldots (4a)$$

Similarly, the time-average of the grain charge $\langle z_p \rangle_t$ is used:

$$\langle z_p \rangle_t = \frac{\sum_{l=1}^{N_t} z_p(t) \Delta t_l}{\sum_{l=1}^{N_t} \Delta t_l} \dots (4b)$$

In the grain scale *corrector* step, the grain is moved according to the solution of respective Langevin equation of motion with a suitable timestep Δt_p (that is different from and much larger than the ion scale timestep Δt_i):

$$m_p \frac{d\vec{v}_p}{dt} = -f_p \vec{v}_p + \vec{F}_p^B + \langle \vec{F}_p \rangle_t + \langle z_p \rangle_t E_0 \dots (5)$$

f_p is the grain friction factor calculated using the Stokes-Cunningham formula [131, 132]. We find the sensitivity of simulation results to the difference in f_p to the Stokes-Cunningham formula (eq. S204) and the more commonly used Epstein's formula[133, 134] (eq. S205) to be negligible. More details are presented in Section S2, SI. At low pressures, eq. S205 may be used and as a generalization, eq. S204 is valid from low to high / atmospheric pressures. $\langle z_p \rangle_t E_0$ is the electric force on the grain. After $M_t = 10000$ timesteps, the simulation is switched to the ion scale again and the grain is frozen at the last known position and is stationary in the ion scale simulation. DRIAD advances the grain motion by one timestep while we do so for M_t timesteps to accelerate convergence.

In total, the predictor step estimates the grain charge and the ion force on the same due to the flowing ions. The corrector step assumes a frozen charge and force due to ions and estimates the grain drift velocity $\langle \vec{v}_p \rangle_t$. The predictor-corrector cycle (**Figure 1**) is repeated until three parameters converge to steady state (time-averaged) values:

1. Force exerted by the ions on the grain $\langle \vec{F}_p \rangle_t$,
2. grain charge $\langle z_p \rangle_t$, and
3. grain drift velocity $\langle \vec{v}_p \rangle_t$.

Experimental parameters were converted to nondimensional form for numerical expediency and time-averaged estimates of observables (such as grain charge $\langle z_p \rangle_t$, drift velocity $\langle \vec{v}_p \rangle_t$, and ion drag force $\langle \vec{F}_p \rangle_t$) from the simulation were converted back to dimensional form for comparison with those from experiments. The equations used to update ion and grain positions and velocities are presented in Section S3 and S4, *SI*, respectively, in nondimensional form. Considerations for the selection of simulation parameters such as the box size, timestep for the ion scale simulation Δt_i and for the grain scale simulation Δt_p, number of ions N_i to ensure that the obtained simulation results do not depend on these choices are summarized in Section S5, *SI*. Section S5 also presents a table showing the insensitivity of simulation results for N_t, M_t values (**Figure 1**) used.

Figure 2 presents time-resolved computations of $z_p(t), \vec{F}_p(t), \vec{v}_p(t)$ for a single grain of radius $a_p = 1.3\,\mu m$ drifting in a DC discharge with $T_e = 5.7\,eV, n_e = 4 \times 10^{14}\,m^{-3}, T_i = 0.03\,eV, p_g = 120\,Pa$ corresponding to a datapoint reported by

Yaroshenko, Ratynskaia, Khrapak, Thoma, Kretschmer, Höfner, Morfill, Zobnin, Usachev, Petrov *et al.* [16]. For this case, $N_i = 1024$ drifting ions were simulated to interact with an isolated grain in a box of side $L^* = 110$. We also conducted the same simulation with $N_i = 2048$ ions in a box of side $L^* = 138$ and found that the results (not presented) are statistically indistinguishable. Panels (A, B), (C, D), (E, F), respectively, present the grain charge, ion drag force, grain velocity in the absence of electric field ($E_0 = 0$ denoted as FIELD OFF) and in presence of electric field ($E_0 = 200\frac{V}{m}$ denoted as FIELD ON). The mean charge $\langle z_p \rangle_t \sim -2645$ when the field is ON (panel A) and $\langle z_p \rangle_t \sim -2684$ when the field is OFF (panel B) agree well with the value (~ 2644) calculated using a simple current balance $I_i^{coll} = I_e^{OML}$ under low field conditions; I_i^{coll} is the isotropic ion current calculated using the experimentally verified model of Suresh, Li, Redmond Go Felipe and Gopalakrishnan [85] and I_e^{OML} is given by eq. 1. This shows that the simulation accurately predicts isotropic ion transport in the absence of electric fields as would be expected. When the field is turned ON, our approach captures the ion and grain dynamics at field strengths encountered in the PK-4 datasets used here for validation. It can be seen from panel C and D that the components of the force are nominally zero along x, y, z directions when the field is OFF and has a non-zero component along x along when ON which we interpret as the ion drag force. Similarly, the grain velocity components have a mean of zero when field is OFF (panel F) and non-zero values when field is ON (panel E). Although Yaroshenko, Ratynskaia, Khrapak, Thoma, Kretschmer, Höfner, Morfill, Zobnin, Usachev, Petrov *et al.* [16] report only the ion drag force and not the grain charge, their estimation is based on the measured grain drift velocity. Under the same experimental conditions and measured grain trajectories, Ratynskaia, Khrapak, Zobnin, Thoma, Kretschmer, Usachev, Yaroshenko, Quinn, Morfill, Petrov *et al.* [116] and Khrapak, Ratynskaia, Zobnin, Usachev, Yaroshenko, Thoma, Kretschmer, Höfner, Morfill, Petrov *et al.* [117] apply a force balance on the grains to estimate the grain charge. In that process, they use a collisionless model for the ion drag force. The average grain drift velocity $\langle \vec{v}_p \rangle_t$ predicted by our simulation agrees excellently with the measured value $\sim 0.0124\frac{m}{s}$ (panel F) to within 0.25% in this instance; a consistency check can also be seen from panel C where the average value of $\vec{v}_p(t)$ is zero along x, y, z directions when the field is OFF. More comparisons across a broad range of conditions discussed under *Results and Discussion*, further confirm the ability of our approach to accurately resolve grain trajectories, the primary observable in complex plasma experiments from which ion drag force or grain charge is estimated, as evidenced by the excellent agreement with measured and predicted average drift velocities. Our validation philosophy is to compare the calculated grain drift velocities to their experimentally observed counterparts. The overall qualitative and quantitative agreement found in drift velocities is used as the basis for interpreting the simultaneously calculated ion drag force $\langle \vec{F}_p \rangle_t$ and grain charge $\langle z_p \rangle_t$ to be physically valid. From among the experimental datasets chosen for comparison, we

compare grain drift velocities $\langle \vec{v}_p \rangle_t$ where they are the primary observable, especially for the PK-4 experiments in microgravity conditions. For experiments to measure the ion drag force, we compare predicted $\langle \vec{F}_p \rangle_t$ directly with the experimentally observed value.

By invoking the mean field potential theory advanced by Baalrud and Daligault [135], $\langle \vec{F}_p \rangle_t$ can be interpreted as the mean force acting on the grain due to the ions averaged over all possible equilibrium configurations of the ions. The ion scale predictor step computes $\langle \vec{F}_p \rangle_t$ according to eq. 4a that averages over the possible *steady state* ion microstates. We do not imply necessarily imply *equilibrium* following a Maxwell-Boltzmann distribution as equivalent to a *steady state* but allow the ion spatial distribution and velocity distribution to self-consistently evolve in response to the applied electric field and ion concentration. $\langle z_p \rangle_t$ also includes the effect of the electric field and space charge on ion transport (we do assume electron transport is not affected by any forces but by only thermal energy in the conditions of interest here as noted before). $\langle \vec{F}_p \rangle_t$ and $\langle z_p \rangle_t$ used in the grain scale corrector step as constants represent an effective potential approximation of the ion drag force and grain charge, respectively, and are used to calculate $\langle \vec{v}_p \rangle_t$ subsequently. The sum $\langle z_p \rangle_t E_0 + \langle \vec{F}_p \rangle_t$ that appears in eq. 5 is the mean force on the grain due to the applied electric field E_0 and the average contributions of the ions $\langle \vec{F}_p \rangle_t$ taking into account their much faster transport timescales in responding to the electric field.

A steady state force balance on the grain (along the direction of $\vec{E}_0 = E_0 \hat{\imath}$) is:

$$\langle \vec{F}_p \rangle_t \cdot \hat{\imath} + \langle z_p \rangle_t E_0 - f_p \langle \vec{v}_p \rangle_t \cdot \hat{\imath} \stackrel{?}{=} 0 \quad \ldots (6)$$

$\langle \vec{F}_p \rangle_t \cdot \hat{\imath}$ is the ion drag force, $\langle z_p \rangle_t E_0$ is the electric force, and $-f_p \langle \vec{v}_p \rangle_t \cdot \hat{\imath}$ is the neutral drag force. We obtain all three forces from the LD simulation, and a useful sanity check here is to ascertain if the values predicted by our simulation would indeed satisfy eq. 6 which is now reduced to an identity. We found that the independently calculated $\langle \vec{F}_p \rangle_t, \langle z_p \rangle_t, \langle \vec{v}_p \rangle_t$ satisfy eq. 6 for every experimental dataset for which we have made predictions and compared against observables for validation.

4. Results and Discussion

Parametric inputs for calculations presented in Figures 3 – 7 are tabulated in Section S6, *SI*. **Figure 3** (Multimedia view) presents comparison between Langevin Dynamics (LD) predictions and experimental data reported by Yaroshenko, Ratynskaia, Khrapak, Thoma, Kretschmer, Höfner, Morfill, Zobnin, Usachev, Petrov *et al.* [16] for two grain radii $0.64\ \mu m$ and $1.25\ \mu m$. In these experiments, the primary observable was the grain drift velocity: experimental data is presented using black triangles with error bars and LD predictions for the drift velocity along the direction of the applied electric field $\langle \vec{v}_k \rangle_t \cdot \hat{\imath}$ are shown using red circles in panels A (for $0.64\ \mu m$) and D (for $1.25\ \mu m$). Using

the measured drift velocity and a charge gradient with gas pressure $\left(\frac{\partial z_p}{\partial p_g}\right)$, the experimenters estimated the ion drag force that is shown in panels B (for $a_p = 0.64\ \mu m$) and E (for $a_p = 1.25\ \mu m$) along with LD predictions for the ion drag force $\langle \vec{F}_p \rangle_t \cdot \hat{\imath}$. In panels C (for $0.64\ \mu m$) and F (for $1.25\ \mu m$), the ratio of prediction to experiment is presented for the drift velocity (blue squares) and the ion drag force (red diamonds). Firstly, panels A and D show that the predictions follow the measured drift velocities closely for both grain sizes in the range of gas pressure examined. The drift velocity measured is captured to within $\pm 20\%$ (panels C and F) in most instances with a few datapoints with higher deviation in the range of $\sim 20 - 40\%$. Overall, the velocity ratios have values in the range of $\sim 0.9 - 1.4$ indicating good agreement with experiment albeit a slight trend of underprediction. We believe the quality of agreement can be improved by using finer timestep but due to high computational times we did not pursue that. In the future, optimization of parallel processing and use of multiple GPUs could enable improvement. We reiterate that the drift velocity is the quantity that was measured unambiguously from the frames recorded during the experimental runs and the overall good agreement seen here indicates high fidelity of our LD simulation approach. The comparison between the ion drag force predictions and estimates reported (panels B and E) are also closely matching each other with the ratio of prediction to experiment is $\sim 0.8 - 1.4$ in most cases (panels C and F) and values at the higher end of pressure are $\sim 1 - 4$. The results presented in **Figure 3** (Multimedia view) were calculated using a fixed simulation box size based on a grain concentration of $10^5\ cm^{-3}$ reported by PK-4 studies published circa ~2005 [16, 114-117]. For each gas pressure, the electron concentration and temperature are estimated using the correlation (reported by these studies) noted in Table S6-A, *SI*. The number of ions used in each simulation run and the box size are estimated based on the dust grain concentration n_p as described in Section S5, *SI*. We also carried out simulations with a fixed number of ions $N_i = 1024$ and $N_i = 2048$ with increasing order of ion population interacting with a single grain (assuming $n_p \to 0$) while maintaining the experimental ion concentrations (by varying the box size suitably) shown in Figures S7-A and S7-B, respectively. Predictions derived using the three sets of N_i (variable, 1024, 2048) will be discussed soon.

Figure 4 presents comparisons between LD predictions and grain charge measurements reported by Khrapak, Ratynskaia, Zobnin, Usachev, Yaroshenko, Thoma, Kretschmer, Höfner, Morfill, Petrov *et al.* [117]. Figure S7-C and S7-D show results derived using $N_i = 1024$ and $N_i = 2048$ ions, respectively, and a variable box size. It is interesting to noted that Yaroshenko, Ratynskaia, Khrapak, Thoma, Kretschmer, Höfner, Morfill, Zobnin, Usachev, Petrov *et al.* [16] and Khrapak, Ratynskaia, Zobnin, Usachev, Yaroshenko, Thoma, Kretschmer, Höfner, Morfill, Petrov *et al.* [117] described analysis on data from the same experimental device, with the former using experimentally measured drift velocities to extract ion drag force and the latter for calculating grain charge

[117] use a force balance such as eq. 6 that assumes a collisionless ion drag model to calculate grain charge using experimentally measured drift velocities. Panels A $(a_p = 0.64\ \mu m)$ and C $(a_p = 1.25\ \mu m)$ show LD predictions and experimentally inferred grain charge in the pressure range $20 - 120\ Pa$. Except at $\sim 20\ Pa$, good agreement to within $\sim 20\%$ (panels B and D). The datapoint at 20 Pa is an outlier for both grain sizes and defies explanation using the collision physics incorporated into our LD simulation. When taken together with the higher-than-average difference observed for drift velocity in **Figure 3** (Multimedia view) at ~20 Pa, we attribute these differences to systemic factors in using Langevin Dynamics approach at low pressures. This explanation requires further examination of the trajectory simulation methodology and incorporation of additional physics into our simulation. It might be advantageous to use larger domain sizes to simulate ions and neutrals explicitly to accurately represent ion orbit formation around individual grains in future work at low pressures.

A single value of dust grain concentration ($n_p = 10^5\ cm^{-3}$) might not be constant for the entire pressure range examined, because at low pressures grain charge is significantly higher compared to high pressures for a given grain radius. Predictions displayed in **Figures 3** and **4** were derived using variable N_i and a fixed box size (based on $n_p = 10^5\ cm^{-3}$). Results derived using variable N_i and fixed number of N_i are seen to be similar for the datasets presented in **Figures 3** and **4**. This could result in lower effective grain density (in the plasma volume that was imaged and from which grain trajectories were recorded) at low pressures due to strong repulsion among the grains as they are more spread out compared to high pressure in which grains could be dispersed at higher effective number concentration, by the same reasoning. The use of a single $n_p = 10^5\ cm^{-3}$ for the entire pressure range leads to variations in the size (number) of the ion population that interact with an individual grain and might also contribute to deviations at low pressures. That was our reason to run the same simulation cases with fixed ion populations of $N_i = 1024$ and $N_i = 2048$ along with variable ion population (and fixed box size) cases to understand how simulation predictions would vary with the size of the ion population. For $a_p = 1.25\ \mu m$ grains, we obtained better agreement at low pressures with $N_i = 2048$ than with $N_i = 1024$ or variable ion population sizes (with fixed box size) while uniformly good agreement is seen at high pressure regardless of the fixed/variable number of ions used in the simulation. If we used the box size calculated based on an ion concentration n_i value at low pressure ($\sim 20\ Pa$) and with $N_i = 2048$ ion population to calculate a grain concentration, we find that this estimate is lower than the reported value ($\sim 10^5\ cm^{-3}$), leading us to construe that the effective grain concentration (that is found in the plasma region imaged during experimental runs) varies with gas pressure. In other words, the effective grain concentration should be ideally *measured* as plasma parameters such as gas pressure, electron number density/temperature are varied and should be individually measured for each experimental run (or for runs with

the same parameters) rather than use a single mean value for the entire range of parameters.

As can be seen from **Figures 3** and **4**, excellent agreement is seen at >~50 Pa limit and motivates comparison with experiments done in the pressure range of ~100 – 500 Pa by Khrapak, Tolias, Ratynskaia, Chaudhuri, Zobnin, Usachev, Rau, Thoma, Petrov, Fortov *et al.* [118]. **Figure 5** presents, in panel A, the measured and LD-computed grain drift velocity (the primary observable). Excellent agreement ~20% is seen as evidenced by the ratio of prediction to experiment presented in panel C. Khrapak, Tolias, Ratynskaia, Chaudhuri, Zobnin, Usachev, Rau, Thoma, Petrov, Fortov *et al.* [118] used a collisionless ion drag model [34] in the grain force balance to infer the grain charge, construed as the measured grain charge. It is seen that a clear disagreement exists between the collisional interpretation offered by LD and the collisionless interpretation used by the original authors. By virtue of the excellent agreement seen for drift velocity, we consider the grain charge calculated by our LD approach to be physically accurate. Even though our validation here only goes up to 500 Pa, considering the increasing exactness of Langevin Dynamics at high pressures [119, 121, 136], the presented LD approach can be also applied for simulating particle behavior in atmospheric or high-pressure plasmas as well. It is instructive to compare LD predictions against prior models of ion drag force [34, 68]. Specifically, we focus on the collisional model derived by Hutchinson and Haakonsen [68] by fitting PIC simulation results as a function of a collisionality parameter that is a function of ion mobility or gas pressure (with the equations used to calculate ion drag presented in Sec. S8, *SI*). We also compute ion drag force according to the collisionless ion drag model derived using the binary collision approach[3, 34, 48, 50, 52, 53] and presented in final form by Khrapak, Ivlev, Morfill and Thomas [34] with an improved approximation for momentum transfer cross-section between an ion and the grain (again, equation is presented in Sec. S8). For clarity, the ion drag force calculated using LD and experimentally measured by Yaroshenko, Ratynskaia, Khrapak, Thoma, Kretschmer, Höfner, Morfill, Zobnin, Usachev, Petrov *et al.* [16] are presented in **Figure 6** along with ion drag force predictions from the models of Hutchinson and Haakonsen [68], Khrapak, Ivlev, Morfill and Thomas [34], and LD simulations (this study). Both these models require an input of the grain charge z_p or surface potential φ_p. φ_p calculated using OML theory for both ions and electrons and using z_p and φ_p calculated simultaneously using LD (that treats ion-neutral collisionality and electrons as collisionless entities) corresponding to the conditions used in **Figure 3** for Hutchinson and Haakonsen [68] model. In addition to these two sets of calculations, φ_p using the collisional ion current model of Suresh, Li, Felipe and Gopalakrishnan [137] is also used for Khrapak, Ivlev, Morfill and Thomas [34] model. These predictions are calculated for each of the two models and presented in **Figure 6** for grain radii $a_p = 0.64, 1.25\ \mu m$. It is clearly seen that the collisional PIC model agrees well with experimental data when φ_p from LD is used than when φ_p calculated using OML is used. This shows that z_p or ϕ_p is strongly influenced by gas pressure, as

expected, and cannot be realistically represented by a collisionless OML model at the pressures of interest here. It is also seen that the collisionless Khrapak, Ivlev, Morfill and Thomas [34] model predicts trends that are in agreement with experimental data, and the predictions of LD and Hutchinson and Haakonsen [68] when φ_p from LD is used than when φ_p calculated using OML or collisional charging model is used. When the charge calculated from our LD approach is used in the chosen prior models, the predictions of ion drag force by the three approaches are qualitatively similar and differ only slightly. The key advantage of the presented LD approach is the handling of the effect of gas pressure on ion trajectories using an implicit representation of neutral drag force on ions and their Brownian motion. The ion drag force calculations and grain charge calculations cannot be treated as separate problems, but two sides of a coin. Our approach simultaneously tracks the charge and momentum transport on to the grain when ions are driven by an applied electric field. As it is well known, OML or current collisional models of ion current do not consider the effect of electric field, while our simulations self-consistently track ion motion, ion flux to the grain, and momentum imparted to the grain by the ions (both long-range and collisional contributions). In both prior approaches [34, 68], the grain charge was calculated separately and used as an input for the ion drag calculations. When OML-derived charge was used or when collisional current-derived charge was used, it is seen that the predictions do not agree with experimental data of Yaroshenko, Ratynskaia, Khrapak, Thoma, Kretschmer, Höfner, Morfill, Zobnin, Usachev, Petrov *et al.* [16]. When LD-computed charge is used, both models agree well with the experimental data. This suggests that the presented approach and prior approaches [34, 68] lead to similar estimates of the ion drag force when the same charge value is used. We construe this as a reasonable demonstration of the ability of LD simulations to reproduce prior experimental data as well as modeling results.

We next present comparisons with the ion drag force measured by Hirt, Block and Piel [14] and Hirt, Block and Piel [15] in **Figure 7** (Multimedia view). This experiment, as noted before, directly measured the ion drag force on spherical grains ($a_p = 10\ \mu m$) using their lateral deflection due to impacts by a transverse ion beam of known kinetic energy and concentration. Thus, in this comparison we obtain a direct test of our simulation's ability to predict the ion drag force at $0.07\ Pa$ (panel A) and $7.2\ Pa$ (panel B) in Argon gas. The ion beam energy was varied in the range of 3 – 45 eV and it was measured by the experimenters that the beam density was 2.5% of the total ion density in the plasma. As mentioned earlier, the use of Langevin Dynamics at high pressures is unambiguous and well-established [136, 138]. For low pressure systems, Langevin Dynamics provides increasingly accurate results when a timescale of interest t_s (simulation or observation time) is much longer than the ion relaxation time t_r (time for the ion velocity distribution function to become Maxwellian through collisions with neutrals) and is appropriate generally when $t_s \gg t_r$, *except* when one is interested in particle transport timescales that are comparable or shorter than the relaxation times [139] ($t_s \ll t_r$). We ran our simulations

to simulate times that are much longer than the ion relaxation time at 0.07 Pa at the lowest beam energy (~0.3 eV) and found that the grain charge and ion drag converge at simulation times that are much shorter than the ion relaxation time. In other words, we find that the ion and electron transport timescales are shorter than t_r. Nevertheless, we ran the simulation for up to $\sim 5t_r$ and found that the simulation results do not vary with the duration of physical time simulated. We refrained from doing this for all the cases at 0.07 Pa as these calculations are computationally expensive and do not reveal additional information. At high pressures, on account of t_r being much shorter than t_s (ion transport to the grain), our runs are all are $\gg 5t_r$ across the board. Firstly, excellent agreement is seen for beam energies > 10 eV. Below 10 eV, we see that the ion drag force prediction is systematically higher than the measured value for a specific reason. Charge exchange (also known as resonant charge transfer) collisions between ions and neutrals, in this case between Ar^+ and Ar, could potentially explain the reduction in ion drag force at low beam energies. Charge exchange collisions replace a fast-moving ion with a slowing moving thermal ion and a slow neutral [140]. This effectively reduces the average momentum collected by the grain from the ion beam as a significant number of fast ions are replaced by slower ones at lower ion beam energies due to larger charge exchange cross section than higher energy beam. Calculations of the charge exchange cross section for Ar^+/Ar are $7.2 \times 10^{-15}, 6.0 \times 10^{-15}, 4.9 \times 10^{-15}\ cm^2$, respectively, at $0.1, 1, 10\ eV$ beam energies [141]. It is expected that the effect of charge exchange collisions on the ion drag force will become weaker at higher beam energies and vice versa [142]. This trend is clear in our simulation predictions wherein our model, which does not account for charge exchange, does well for high beam energies and is seen to systematically over-predict the force at lower energies. In future work, we plan to attempt to include the effect of charge exchange cross-sections into the LD simulation using a Monte-Carlo approach and improve the accuracy of the same. Overall, our LD approach is seen to accurately compute ion drag force in this comparison [14, 15], grain velocity in the comparison with Yaroshenko, Ratynskaia, Khrapak, Thoma, Kretschmer, Höfner, Morfill, Zobnin, Usachev, Petrov *et al.* [16], and grain charge in comparison with Khrapak, Ratynskaia, Zobnin, Usachev, Yaroshenko, Thoma, Kretschmer, Höfner, Morfill, Petrov *et al.* [117].

In summary, the ability to track a large number of ions efficiently is an advantage of using LD and the presented approach is well-suited for simulating plasmas at pressures >~20 Pa wherein the ion and grain trajectories are strongly influenced by collisions with neutrals that leads to neutral drag and Brownian diffusion. LD captures the scattering or randomization of ion momentum via the stochastic Brownian force $\vec{F}_B$ and is exact in the limit of high pressures[136, 138]. At low pressures (<~20 Pa), the long-range ion orbits around grains are minimally influenced by collisions with neutrals. The accuracy and suitability of the presented LD approach for this regime remains to be further examined in future work at low pressures. Specifically, accurately resolving ion orbital motion at low pressures, in

addition to ion drift/streaming towards a grain and ion thermal motion, would require larger simulation domain sizes as was demonstrated by the construction of prior PIC codes such as SCEPTIC [55-57], and the incorporation of charge exchange collisions to accurately track the velocity distribution of the simulated ions in collisional plasma flows at low pressures interacting with a grain. We construe that such an approach could potentially incorporate the predictor-corrector iteration scheme with a PIC-based trajectory simulation method (such as SCEPTIC) to advance the ion trajectories without invoking superion constructs. Simulating ion motion around an individual grain at low pressures using SCEPTIC (or equivalent PIC codes) would allow calculation of the grain charge and ion drag force at the scale of an individual grain. As demonstrated here, the calculated grain charge and ion drag force, when incorporated into the grain scale equations of motion, would allow prediction of the grain trajectory / drift velocity and direct comparison with complex plasma experiments, typically conducted at pressures <10 Pa to observe collective behavior of charged grains. The presented predictor-corrector approach could potentially be used with PIC codes to calculate ion trajectories at low pressure and a Langevin Dynamics formulation (similar to here) can be retained to simulate the grain drift velocities/trajectories for direct comparison with complex plasma experiments. An experiment of interest would be to trap and observe the steady-state drift of a single grain in a complex plasma that can be exactly compared with the predictions of our code as well as with prior PIC codes such as SCEPTIC. Complex plasma experiments typically involve multiple, and often numerous, grains that interact with each other electrostatically and influence each other's trajectories and ion collection (charge). Any simulation of multiple grains would also need careful characterization of the number density in pertinent experiments to allow appropriate comparisons.

5. Conclusions

The presented simulation methodology and comparisons with experimental data allow the direct numerical simulation of ion and grain trajectories in a two-temperature plasma containing hot electrons and all other species at room temperature. We utilize comparisons of predictions with an observable in a complex plasma experiment, namely, the time-averaged grain velocities and ion drag force reported by Yaroshenko, Ratynskaia, Khrapak, Thoma, Kretschmer, Höfner, Morfill, Zobnin, Usachev, Petrov *et al.* [16], the ion drag force reported by Hirt, Block and Piel [14] and Hirt, Block and Piel [15], and the grain charge reported by Khrapak, Ratynskaia, Zobnin, Usachev, Yaroshenko, Thoma, Kretschmer, Höfner, Morfill, Petrov *et al.* [117] and Khrapak, Tolias, Ratynskaia, Chaudhuri, Zobnin, Usachev, Rau, Thoma, Petrov, Fortov *et al.* [118], to establish the physical validity and accuracy of our predictor-corrector Langevin Dynamics ion and grain trajectory simulation approach. In each instance of our comparisons, we have specified the physical inputs to our calculations such as plasma discharge parameters, gas

conditions, and grain size as well as considerations for selecting simulation parameters. From this modeling study, we derive the following conclusions:

1. Complex plasmas are a unique experimental system that allows kinematic resolution of grain trajectories. To obtain insights about the behavior of ion transport (charging kinetics) and momentum exchange with grains (ion drag force), we have presented an experimentally validated self-consistent simulation method that draws ideas and inspiration from prior approaches [55, 72, 78] and addresses conceptual and computational challenges with the same to yield a robust method to study ion and grain dynamics at tractable computational expenses.
2. Ion trajectories and their spatial distribution in the presence of charged grains are of interest in the study of dusty plasmas and our methodology could be potentially effective in visualizing the space charge effect and multi-body electrostatic interactions in low-temperature complex plasmas. Along with this article, we present several animations of grain-ion interactions that illustrate the effect of grain size, gas pressure, ion beam energy as described in Section S8, *SI*.
3. Our approach is amenable to the incorporation of ion, electron, and grain physics that were not included in the current study. Specifically, the effect of charge exchange collisions on the ion drag force remains to be probed, both computationally and experimentally. The excellent agreement obtained in our comparisons with the data reported by Hirt, Block and Piel [14] and Hirt, Block and Piel [15] at high beam energies show promise of our approach to capture the ion drag force accurately. At low beam energies, wherein charge exchange is expected to be significant, modeling of the ion in our simulation (using eq. 2) as an entity whose velocity may be randomized based on the outcome of a Monte Carlo charge exchange operator (that takes into account the charge exchange cross-section between the ion and the neutral gas molecules) is an obvious extension of the presented approach that could lead to improved agreement in the future. In addition to improving approximations pertaining to the ions and electrons, the grain shape could also be easily generalized to computationally study the effect of non-spherical grain morphology on charging kinetics and ion drag force.
4. The overall good agreement seen here between experimental data and the predictions of the presented LD-based approach establish to simulate grain behavior at high pressures (>~20 Pa) wherein collisions between ions and neutral gas molecules cause neutral drag on and Brownian motion of the ions, and charge exchange is less important. This culminates in ion drift without significant orbit formation. Further work is necessary to explore using larger simulation domain sizes to accurately simulate ion trajectories at low pressures (<~20 Pa) wherein long-range ion orbits around the grain are significant. Nevertheless, the presented LD-based approach addresses a need to accurately predict charging, ion drag, and grain trajectories at high pressures. This is of potential utility in modeling grain dynamics in low-temperature process

plasmas used for nanomaterials synthesis [143, 144], surface treatment [145], to name a few.

5. In this study, we focused on validating our approach for the case of ion transport at relatively low or dilute dust grain concentrations and included exactly one grain in our simulations. Charged by ion and electron transport processes, typically of the order of μs, grains exhibit interesting cooperative dynamics in ms timescales that has spawned the field of complex plasmas as an analogue of classical matter to study condensed matter physics, fluid dynamics, statistical physics, to name a few. The predictor-corrector approach presented here could be readily extended to simulate the interaction of a charged grain with external fields without prescribing their charge *apriori*. In the current study, grain charge is self-consistently calculated using the ion scale simulation and used to capture the dust dynamics in the grain scale step. The iteration between the two scales leads to reliable convergence of the grain observables. Although the present approach does not consider experiment-specific electric field or plasma chamber geometries, it is nevertheless valid for simulating electrostatic interactions in regions near the center of dust clouds wherein effect of confinement and other non-uniformities vanish. Thus, the presented approach can be developed as a Low-Temperature Complex Plasma Simulator (LTCPS). After further validation against experiments that probe the effect of ion concentration, externally applied electric and/or magnetic fields, and plasma discharge parameters, such a LTCPS advanced here could be a potentially useful dusty plasma research and pedagogical tool.

Supplemental Material (SI)

Section S1. Electron velocity distribution function and current to grain with and without electric field

Section S2. Equations used to calculate ion and particle friction factor

Section S3. Equations used to advance position and velocity of ion (predictor step)

Section S4. Equations used to advance position and velocity of grain (corrector step)

Section S5. Simulation timestep and box size selection considerations

Section S6. Tabulations of the inputs used for obtaining predictions presented in Figures 3 – 5 of the main text

Section S7. Additional plots that accompany Figures 3 and 4 of the main text

Section S8. Description of ion trajectory animations accompanying this article

Section S9. Equations of prior ion drag models

Acknowledgements

Funding for this research was provided by US National Science Foundation Plasma Physics Award 1903432 from the Directorate of Physical and Mathematical Sciences, US Department of Energy FY2020 Early Career Award DE-SC0021106 from the Office of Fusion Energy Sciences and Award DE-SC0021246 from the Office of Basic Energy Sciences, US Army Research Office Award W911NF-23-2-0013 from the Sciences of Extreme Materials Branch. Computational resources were provided by The University of Memphis High Performance Computing Center and NSF Discover ACCESS Allocation PHY220140.

Conflicts of Interest

The authors have no conflicts to disclose.

Data Availability Statement

The data that support the findings of this study are available from the corresponding author upon reasonable request.

Table 1: Summary of the SCEPTIC, MAD, and DRIAD codes

	SCEPTIC	MAD	DRIAD
Nature of entities simulated	Ions of charge Ze	Superions that represent several ions that have the same charge to mass ratio	Same as MAD
Electron number concentration	Retain the Boltzmann factor $e^{\frac{e\varphi_p}{k_B T_e}}$ in the Poisson equation for φ_p	Present grain-superion interaction as bare Coulombic and superion-superion interaction as shielded Coulombic with $\lambda_{D_e} \sim n_{e\infty}^{-\frac{1}{2}}$	Same as MAD
Ion-neutral collisions	Included using a Monte Carlo approach to mimic ion-neutral momentum scattering	Not included	Collision force is included as a thermal bath force that randomizes ion momentum
Grain motion	Grain is assumed to be static	Grain is assumed to be static	Grain motion is advanced using a suitable timestep while keeping the ions frozen; iterative convergence obtained
Major drawbacks	Solving the non-linear Poisson equation after each timestep involves meshing around the grain and renders the dynamic tracking of grain motion difficult. Including ion-neutral collisions by only randomizing the ion momentum fails to include the drag experienced by ions due to relative motion with respect to the gas.	Superion is a construct that compresses the spatial distribution of several ions to a point while maintaining only their charge to mass ratio. Suitable only for simulating ion flows at very low pressure in which ions do not collide with neutrals.	Superion is a construct that compresses the spatial distribution of several ions to a point while maintaining only their charge to mass ratio. Including ion-neutral collisions by only randomizing the ion momentum fails to include the drag experienced by ions due to relative motion with respect to the gas.

Table 2: Studies reporting measurements of ion drag force or grain charge on spherical grains immersed in complex plasmas and relevant (nominal) experimental conditions. Those shown in **bold** are used for validation in this study.

Reference	$n_e(m^{-3})$	$T_e(eV)$	$d_p(\mu m)$	Gas pressure, others
Zafiu, Melzer and Piel [12]: The total force on free falling microspheres is shown to be the sum of the ion drag force, thermophoretic force, and the electric force.	$\sim 4 \times 10^{15}$	6	9.55	He (100 – 200 Pa), electric potential and temperature profile reported.
Zafiu, Melzer and Piel [13]: Ratio of the ion drag force to electric force measured on free falling microspheres	$\sim 4 \times 10^{15}$	4 at low pressure, 6 at high pressure	3.47, 4.8, 7.1, 12.1	He (20 – 200 Pa), electric potential and temperature profile reported.
Fortov, Petrov, Usachev and Zobnin [146]: Grain charge on free falling microspheres	$\sim (3-4) \times 10^{14}$	$3.5-4.5$	1.80, 12.74	Ne (20 – 50 Pa), electric field $E_0 \sim 200 \frac{V}{m}$
Hirt, Block and Piel [15]: Ion drag force on free falling microspheres due to ion beams due to a DC discharge.	$\sim 10^{14}-10^{16}$	$2-4$	20	Ar (10^{-2} – 10^{-1} Pa), ion beam energy $U_0 \sim 3-45$ eV, ion beam density $n_B \sim 10^{13}-10^{15}$ m^{-3}
Hirt, Block and Piel [14]: Ion drag force on free falling microspheres due to ion beams due to a DC discharge.	$\sim 10^{14}-10^{16}$	$2-4$	19	Ar (7.2 Pa), ion beam energy $U_0 \sim 3-45$ eV, ion beam density $n_B \sim 10^{13}-10^{15}$ m^{-3}
Ratynskaia, Khrapak, Zobnin, Thoma, Kretschmer, Usachev, Yaroshenko, Quinn,	$\sim (1.5-4) \times 10^{14}$	$5-8$	0.64, 1.3	Ne (20 – 120 Pa), electric field $E_0 \sim 200 \frac{V}{m}$

Morfill, Petrov *et al.* [116]: Grain charge on microspheres dispersed in a DC discharge formed in the PK4 chamber in microgravity conditions.				
Khrapak, Ratynskaia, Zobnin, Usachev, Yaroshenko, Thoma, Kretschmer, Höfner, Morfill, Petrov *et al.* [117]: Grain charge on microspheres dispersed in a DC discharge formed in the PK4 chamber in microgravity conditions.	$\sim(1.5-4)\times10^{14}$	$5-8$	0.6, 1.0, 1.3	Ne $(20-120\ Pa)$, electric field $E_0{\sim}200\frac{V}{m}$
Yaroshenko, Ratynskaia, Khrapak, Thoma, Kretschmer, Höfner, Morfill, Zobnin, Usachev, Petrov *et al.* [16] reporting ion drag force and Yaroshenko, Ratynskaia, Khrapak, Thoma, Kretschmer and Morfill [17] reporting dust-ion momentum transfer frequency on microspheres dispersed in a DC discharge formed in the PK4 chamber in microgravity conditions.	$\sim(1.5-4)\times10^{14}$	$5-8$	0.64, 1.3	Ne $(20-120\ Pa)$, electric field $E_0{\sim}200\frac{V}{m}$
Nosenko, Fisher, Merlino, Khrapak, Morfill and Avinash [18]: Ion drag force on free falling microspheres due to a DC discharge.	$\sim(0.4-2.7)\times10^{16}$	$\sim1.4-2$	40, 59	Ar $(\sim0.08\ Pa)$, electric field $E_0{\sim}0.9-4.4\frac{V}{m}$
Khrapak, Tolias, Ratynskaia, Chaudhuri, Zobnin, Usachev, Rau, Thoma, Petrov, Fortov *et al.*	$\sim(5-12)\times10^{14}$	$\sim4-8$	1.3	Ne $(100-500\ Pa)$, electric field $E_0{\sim}200\frac{V}{m}$

[118]: Grain charge on microspheres dispersed in a DC discharge formed in the PK4 chamber in microgravity conditions.				
Beckers, Trienekens and Kroesen [19]: Ion drag force on microspheres trapped at the end of the dust free region in a RF discharge in gravity and microgravity conditions.	$\sim 7 \times 10^{14}$	~ 2	~ 4.90	Ar ($\sim 20\ Pa$)
Khrapak, Thoma, Chaudhuri, Morfill, Zobnin, Usachev, Petrov and Fortov [20]: Grain drift velocity on microspheres in a DC discharge in the PK4 chamber in ground and microgravity conditions.	$\sim (1.5 - 4) \times 10^{14}$	$5 - 8$	1.2, 2.55, 3.43	Ne ($20 - 120\ Pa$), electric field $E_0 \sim 200 \frac{V}{m}$
Hall and Thomas [21]: Ion drag force on microspheres in a DC discharge in ground-based experiments.	$\sim 10^{15}$	$3 - 5$	2	Ar ($\sim 24 - 60\ Pa$), electric field $E_0 \sim 0 - 400 \frac{V}{m}$
Antonova, Khrapak, Pustylnik, Rubin-Zuzic, Thomas, Lipaev, Usachev, Molotkov and Thoma [22]: Grain drift velocity and charge on microspheres in a DC discharge in the PK4 chamber in microgravity conditions.	$\sim (1.5 - 4) \times 10^{14}$ in Ne, $\sim (3 - 4) \times 10^{14}$ in Ar	$\sim 5 - 8$ in Ne, $\sim 4 - 5$ in Ar	3.4	Ne ($\sim 20 - 100\ Pa$), Ar ($\sim 20 - 60\ Pa$), electric field $E_0 \sim 200 \frac{V}{m}$

Figure 1: Illustration of the predictor-corrector iteration between ion and grain scales until convergence of grain drift velocity, charge, and ion drag force. At steady state, the quantities indicated in red are obtained from the Langevin Dynamics (LD) simulation and are checked if they satisfy the force balance on a single grain. The grain drift velocity $\langle \vec{v}_p \rangle_{drift}$ is compared with its experimental counterpart wherever available. In other instances, the grain charge z_p or the ion drag force $\vec{F}_{id}$ are compared with appropriate experimental data.

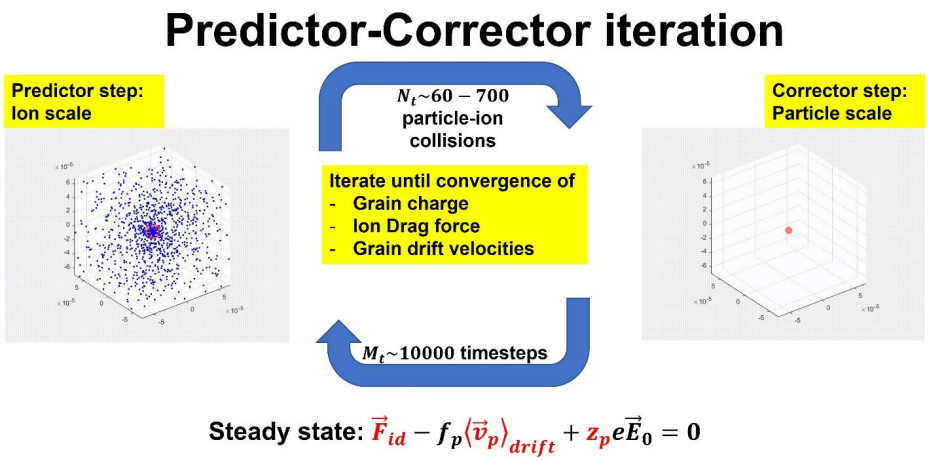

Figure 2: Representative calculations using the presented predictor-corrector trajectory simulation approach for $1.3\ \mu m$ grains immersed in a DC discharge under conditions that are typical of the PK-4 experiment $\left(E_0 = 200\frac{V}{m}\right)$.

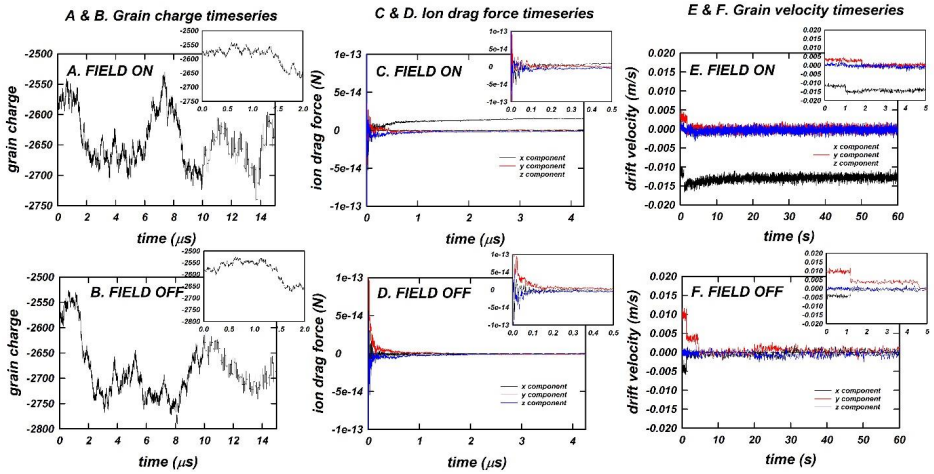

Figure 3 (Multimedia view)**:** Comparisons between LD predictions and experimental data reported by Yaroshenko, Ratynskaia, Khrapak, Thoma, Kretschmer, Höfner, Morfill, Zobnin, Usachev, Petrov *et al.* [16]. Shown in panels A (drift velocity), B (ion drag force), and C (ratio of simulation to experimental value of drift velocity and ion drag force) for $a_p = 0.64\ \mu m$ grains. Similarly, panels D, E, F are for $a_p = 1.25\ \mu m$ grains.

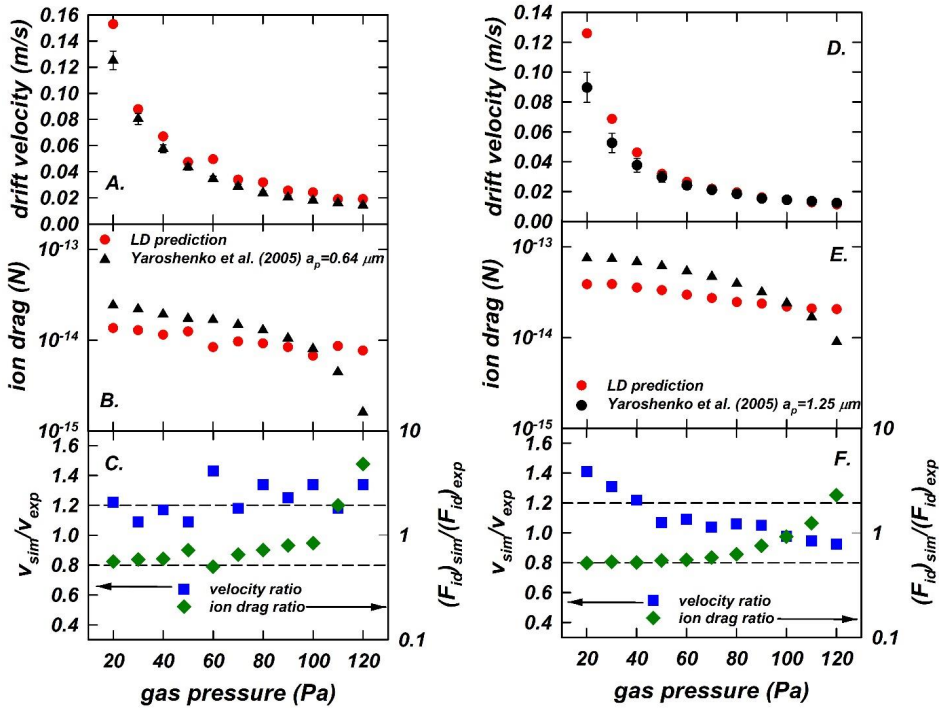

Figure 4: Comparisons between LD predictions and experimental data reported by Khrapak, Ratynskaia, Zobnin, Usachev, Yaroshenko, Thoma, Kretschmer, Höfner, Morfill, Petrov *et al.* [117]. Shown in panel A is (grain charge) and panel B is the ratio of simulation to experimental value of grain charge for $a_p = 0.64\ \mu m$ grains. Similarly, panels C, D are for $a_p = 1.25\ \mu m$ grains.

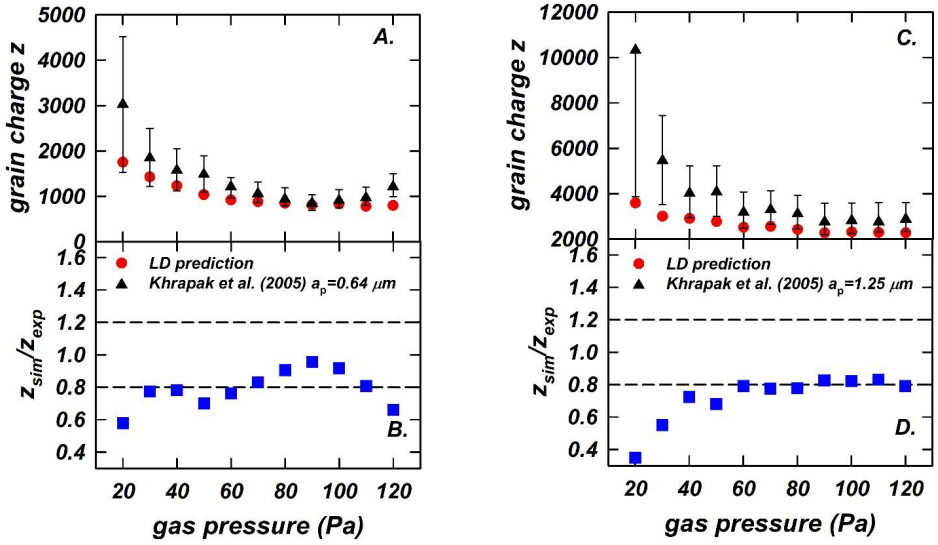

Figure 5: Comparisons between LD predictions and experimental data reported by Khrapak, Tolias, Ratynskaia, Chaudhuri, Zobnin, Usachev, Rau, Thoma, Petrov, Fortov *et al.* [118]. Grain drift velocity is shown in panel A, panel B displays the grain charge, and panel C shows the ratio of simulation to experimental value of grain charge for $a_p = 0.64\ \mu m$ grains. The common legend for panels A and B are noted at the top of the figure and panel C has a separate legend.

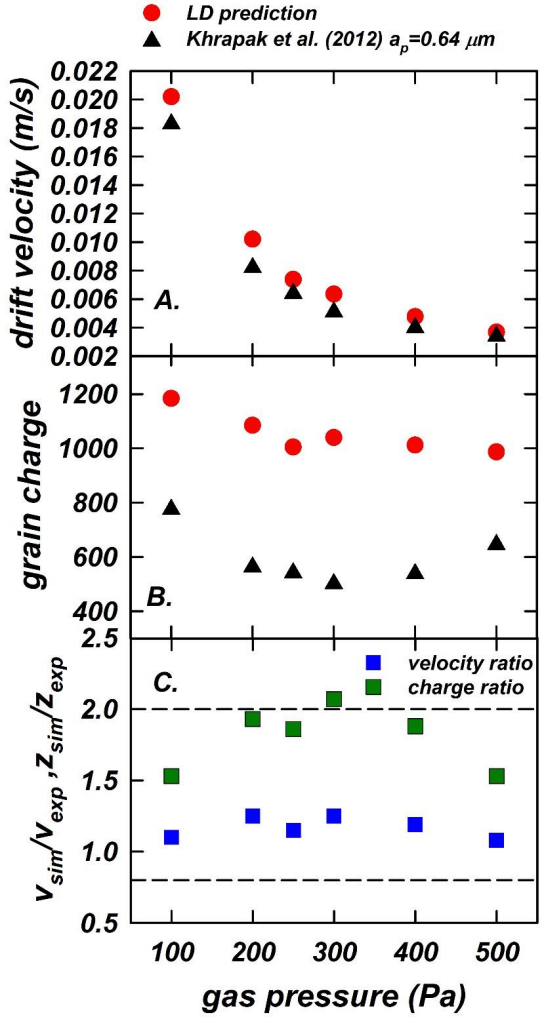

Figure 6: Comparison of ion drag force computed by LD simulations (presented in Figure 3) and predictions of the same using the collisional ion drag model of Hutchinson and Haakonsen [68] derived by fitting PIC simulation results and the collisionless ion drag model of Khrapak, Ivlev, Morfill and Thomas [34]. For Hutchinson and Haakonsen [68] model, two sets of calculations are plotted. One using the grain charge or grain floating potential φ_p calculated using OML[91] current for both ions and electrons and the other using grain charge from LD (this study). For Khrapak, Ivlev, Morfill and Thomas [34], similarly, three values of charge are used: φ_p computed using model of collision enhanced current for the ions[137] and OML current for electrons, φ_p using grain charge z_p using LD (this study), and φ_p using a collisional ion current[137] and OML electron current. Panels A and B present comparisons for grains of radii 0.64 and 1.25 μm, respectively.

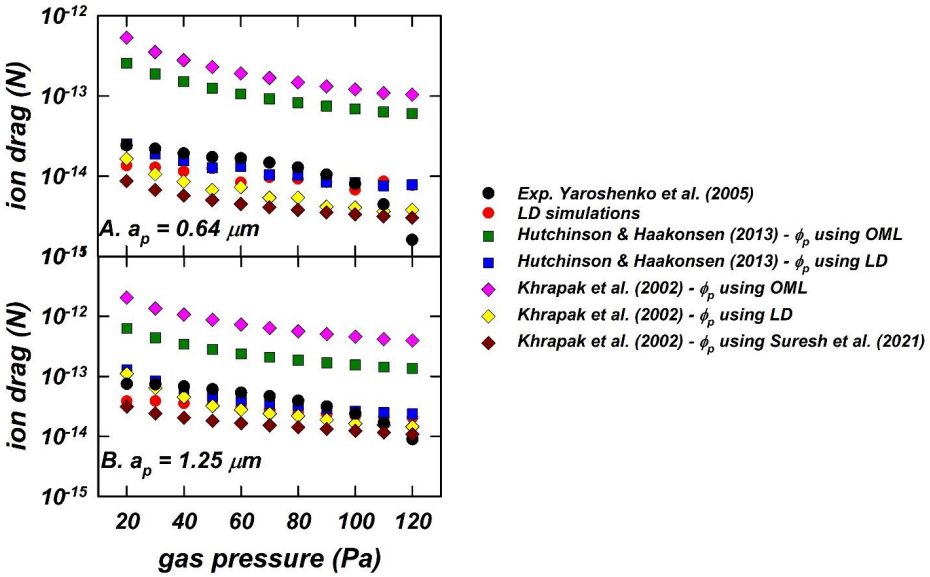

Figure 7 (Multimedia view)**:** Comparisons between LD predictions and experimental data reported by Hirt, Block and Piel [14] and Hirt, Block and Piel [15]. the ion drag force is presented in panel A for 0.7 Pa pressure and in panel B for 7.2 Pa. in both cases, the grains $10\ \mu m$ in radius.

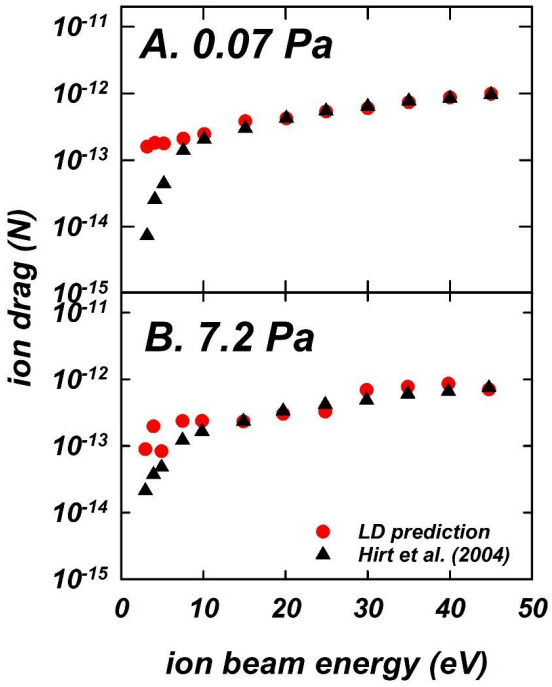

References

[1] V. E. Fortov, A. V. Ivlev, S. A. Khrapak, A. G. Khrapak, and G. E. Morfill, Physics Reports **421** (2005) 1.
[2] S. Khrapak, and G. Morfill, Contrib. Plasma Phys. **49** (2009) 148.
[3] A. V. Ivlev, S. K. Zhdanov, S. A. Khrapak, and G. E. Morfill, Plasma Physics and Controlled Fusion **46** (2004) B267.
[4] G. E. Morfill, and A. V. Ivlev, Reviews of Modern Physics **81** (2009) 1353.
[5] G. Morfill, and H. Kersten, New Journal of Physics **5** (2003) 001.
[6] N. D'Angelo, Physics of Plasmas **5** (1998) 3155.
[7] K. Avinash, Physics of Plasmas **8** (2000) 351.
[8] G. I. Sukhinin, A. V. Fedoseev, M. V. Salnikov, S. N. Antipov, O. F. Petrov, and V. E. Fortov, EPL (Europhysics Letters) **103** (2013) 35001.
[9] J. Goree, G. E. Morfill, V. N. Tsytovich, and S. V. Vladimirov, Physical Review E **59** (1999) 7055.
[10] V. N. Tsytovich, S. V. Vladimirov, G. E. Morfill, and J. Goree, Physical Review E **63** (2001) 056609.
[11] A. M. Lipaev, S. A. Khrapak, V. I. Molotkov, G. E. Morfill, V. E. Fortov, A. V. Ivlev, H. M. Thomas, A. G. Khrapak, V. N. Naumkin, A. I. Ivanov, S. E. Tretschev *et al.*, Physical Review Letters **98** (2007) 265006.
[12] C. Zafiu, A. Melzer, and A. Piel, Physics of Plasmas **9** (2002) 4794.
[13] C. Zafiu, A. Melzer, and A. Piel, Physics of Plasmas **10** (2003) 1278.
[14] M. Hirt, D. Block, and A. Piel, Physics of Plasmas **11** (2004) 5690.
[15] M. Hirt, D. Block, and A. Piel, IEEE Transactions on Plasma Science **32** (2004) 582.
[16] V. Yaroshenko, S. Ratynskaia, S. Khrapak, M. H. Thoma, M. Kretschmer, H. Höfner, G. E. Morfill, A. Zobnin, A. Usachev, O. Petrov, and V. Fortov, Physics of Plasmas **12**, 093503 (2005) 093503.
[17] V. V. Yaroshenko, S. Ratynskaia, S. A. Khrapak, M. H. Thoma, M. Kretschmer, and G. E. Morfill, Contrib. Plasma Phys. **45** (2005) 223.
[18] V. Nosenko, R. Fisher, R. Merlino, S. Khrapak, G. Morfill, and K. Avinash, Physics of Plasmas **14** (2007) 103702.
[19] J. Beckers, D. J. M. Trienekens, and G. M. W. Kroesen, Physical Review E **88** (2013)
[20] S. A. Khrapak, M. H. Thoma, M. Chaudhuri, G. E. Morfill, A. V. Zobnin, A. D. Usachev, O. F. Petrov, and V. E. Fortov, Physical Review E **87** (2013) 063109.
[21] T. H. Hall, and E. Thomas, Ieee Transactions on Plasma Science **44** (2016) 463.
[22] T. Antonova, S. A. Khrapak, M. Y. Pustylnik, M. Rubin-Zuzic, H. M. Thomas, A. M. Lipaev, A. D. Usachev, V. I. Molotkov, and M. H. Thoma, Physics of Plasmas **26** (2019) 113703.
[23] J. Goree, Plasma Sources Science and Technology **3** (1994) 400.
[24] I. Denysenko, M. Y. Yu, L. Stenflo, and N. A. Azarenkov, Physics of Plasmas **12** (2005)
[25] L. Patacchini, I. H. Hutchinson, and G. Lapenta, Physics of Plasmas **14**, 062111 (2007)
[26] K. Matyash, M. Fröhlich, H. Kersten, G. Thieme, R. Schneider, M. Hannemann, and R. Hippler, Journal of Physics D: Applied Physics **37** (2004) 2703.
[27] D. Primetzhofer, M. Spitz, E. Taglauer, and P. Bauer, Surface Science **605** (2011) 1913.
[28] J. Tharamel, V. A. Kharchenko, and A. Dalgarno, Physical Review A **50** (1994) 496.
[29] S. E. Butler, and A. Dalgarno, The Astrophysical Journal **241** (1980) 838.
[30] M. Chaudhuri, S. A. Khrapak, and G. E. Morfill, Physics of Plasmas **15**, 053703 (2008)
[31] S. A. Khrapak, and G. E. Morfill, Physical Review E **69** (2004) 066411.
[32] S. A. Khrapak, M. Chaudhuri, and G. E. Morfill, IEEE Transactions on Plasma Science **37** (2009) 487.
[33] S. A. Khrapak, A. V. Ivlev, G. E. Morfill, and S. K. Zhdanov, Physical Review Letters **90**, 225002 (2003)
[34] S. A. Khrapak, A. V. Ivlev, G. E. Morfill, and H. M. Thomas, Physical Review E **66**, 046414 (2002)
[35] M. D. Kilgore, J. E. Daugherty, R. K. Porteous, and D. B. Graves, Journal of Applied Physics **73** (1993) 7195.

[36] M. S. Barnes, J. H. Keller, J. C. Forster, J. A. O'Neill, and D. K. Coultas, Physical Review Letters **68** (1992) 313.
[37] A. A. Uglov, and A. G. Gnedovets, Plasma Chemistry and Plasma Processing **11** (1991) 251.
[38] H. s. Hahn, E. A. Mason, and F. J. Smith, The Physics of Fluids **14** (1971) 278.
[39] S. A. Khrapak, A. V. Ivlev, G. E. Morfill, S. K. Zhdanov, and H. M. Thomas, IEEE Transactions on Plasma Science **32** (2004) 555.
[40] Y.-D. Jung, Physics Letters A **325** (2004) 279.
[41] V. N. Tsytovich, U. de Angelis, A. V. Ivlev, G. E. Morfill, and S. A. Khrapak, Physics of Plasmas **12**, 092106 (2005)
[42] D. M. Chang, W. S. Chang, and Y. D. Jung, Journal of Applied Physics **99** (2006)
[43] I. Denysenko, K. Ostrikov, and N. A. Azarenkov, Physics of Plasmas **16** (2009)
[44] D. H. Ki, and Y. D. Jung, Applied Physics Letters **97** (2010)
[45] S. A. Khrapak, Physics of Plasmas **21**, 044506 (2014)
[46] I. L. Semenov, S. A. Khrapak, and H. M. Thomas, Physics of Plasmas **24**, 033710 (2017)
[47] S. A. Khrapak, A. V. Ivlev, S. K. Zhdanov, and G. E. Morfill, Physics of Plasmas **12** (2005) 042308.
[48] A. V. Ivlev, S. K. Zhdanov, S. A. Khrapak, and G. E. Morfill, Physical Review E **71** (2005) 016405.
[49] I. L. Semenov, A. G. Zagorodny, and I. V. Krivtsun, Physics of Plasmas **20** (2013) 013701.
[50] S. Khrapak, A. Ivlev, S. Zhdanov, and G. Morfill, in *IEEE International Conference on Plasma Science*2004), p. 431.
[51] S. A. Khrapak, S. K. Zhdanov, A. V. Ivlev, and G. E. Morfill, Journal of Applied Physics **101** (2007) 033307.
[52] S. A. Khrapak, V. Nosenko, G. E. Morfill, and R. Merlino, Physics of Plasmas **16** (2009) 044507.
[53] S. A. Khrapak, A. V. Ivlev, S. K. Zhdanov, and G. E. Morfill, Physics of Plasmas **12**, 042308 (2005)
[54] A. V. Ivlev, S. A. Khrapak, S. K. Zhdanov, G. E. Morfill, and G. Joyce, Physical Review Letters **92** (2004) 205007.
[55] I. H. Hutchinson, Plasma Physics and Controlled Fusion **44** (2002) 1953.
[56] I. H. Hutchinson, Plasma Physics and Controlled Fusion **45** (2003) 1477.
[57] I. H. Hutchinson, Plasma Physics and Controlled Fusion **47** (2005) 71.
[58] I. H. Hutchinson, Plasma Physics and Controlled Fusion **48** (2006) 185.
[59] I. V. Schweigert, A. L. Alexandrov, and F. M. Peeters, IEEE Transactions on Plasma Science **32** (2004) 623.
[60] I. H. Hutchinson, and L. Patacchini, Physics of Plasmas **14**, 013505 (2007)
[61] L. Patacchini, and I. H. Hutchinson, Physical Review Letters **101** (2008) 025001.
[62] I. H. Hutchinson, and L. Patacchini, Plasma Physics and Controlled Fusion **52**, 124005 (2010)
[63] I. H. Hutchinson, Physical Review Letters **107**, 095001 (2011)
[64] L. Patacchini, and I. H. Hutchinson, Plasma Physics and Controlled Fusion **53**, 065023 (2011)
[65] L. Patacchini, and I. H. Hutchinson, Plasma Physics and Controlled Fusion **53**, 025005 (2011)
[66] I. H. Hutchinson, Physical Review E **85**, 066409 (2012)
[67] I. H. Hutchinson, Plasma Physics and Controlled Fusion **55**, 115014 (2013)
[68] I. H. Hutchinson, and C. B. Haakonsen, Physics of Plasmas **20** (2013)
[69] V. R. Ikkurthi, K. Matyash, A. Melzer, and R. Schneider, Physics of Plasmas **16** (2009)
[70] V. R. Ikkurthi, K. Matyash, A. Melzer, and R. Schneider, Physics of Plasmas **17** (2010)
[71] S. Sundar, and Z. A. Moldabekov, Physical Review E **99** (2019) 063202.
[72] A. Piel, Physics of Plasmas **24** (2017) 033712.
[73] J. Wilms, and A. Piel, Physics of Plasmas **24**, 083703 (2017)
[74] P. Ludwig, H. Jung, H. Kählert, J. P. Joost, F. Greiner, Z. Moldabekov, J. Carstensen, S. Sundar, M. Bonitz, and A. Piel, European Physical Journal D **72**, 82 (2018)

[75] W. J. Miloch, H. Jung, D. Darian, F. Greiner, M. Mortensen, and A. Piel, New Journal of Physics **20**, 073027 (2018)
[76] A. Piel, F. Greiner, H. Jung, and W. J. Miloch, Physics of Plasmas **25** (2018) 083702.
[77] A. Piel, H. Jung, and F. Greiner, Physics of Plasmas **25** (2018) 083703.
[78] L. S. Matthews, D. L. Sanford, E. G. Kostadinova, K. S. Ashrafi, E. Guay, and T. W. Hyde, Physics of Plasmas **27** (2020) 023703.
[79] K. S. Ashrafi, R. Yousefi, M. Chen, L. S. Matthews, and T. W. Hyde, Phys Rev E **102**, 043210 (2020) 043210.
[80] S. A. Khrapak, AIP Conference Proceedings **1188** (2009) 83.
[81] L. G. D'Yachkov, A. G. Khrapak, S. A. Khrapak, and G. E. Morfill, Physics of Plasmas **14**, 042102 (2007)
[82] A. G. Khrapak, L. G. D'Yachkov, and S. A. Khrapak, in *AIP Conference Proceedings*2008), pp. 253.
[83] M. Gatti, and U. Kortshagen, Physical Review E **78** (2008) 046402.
[84] A. V. Zobnin, A. P. Nefedov, V. A. Sinel'shchikov, and V. E. Fortov, Journal of Experimental and Theoretical Physics **91** (2000) 483.
[85] V. Suresh, L. Li, J. Redmond Go Felipe, and R. Gopalakrishnan, Journal of Physics D: Applied Physics **54** (2021) 275205.
[86] H. S. Chahl, and R. Gopalakrishnan, Aerosol Science and Technology **53** (2019) 933.
[87] R. Gopalakrishnan, and C. J. Hogan, Physical Review E **85** (2012) 026410.
[88] A. V. Zobnin, A. D. Usachev, O. F. Petrov, and V. E. Fortov, Physics of Plasmas **15** (2008) 043705.
[89] M. Lampe, R. Goswami, Z. Sternovsky, S. Robertson, V. Gavrishchaka, G. Ganguli, and G. Joyce, Physics of Plasmas **10** (2003) 1500.
[90] V. I. Tarasov, and M. S. Veshchunov, Aerosol Science and Technology **52** (2018) 740.
[91] J. E. Allen, Phys. Scr. **45** (1992) 497.
[92] H. M. Mott-Smith, and I. Langmuir, Physical Review **28** (1926) 727.
[93] I. H. Hutchinson, and L. Patacchini, Physics of Plasmas **14** (2007) 013505.
[94] O. S. Vaulina, A. Y. Repin, and O. F. Petrov, Plasma Physics Reports **32** (2006) 485.
[95] N. A. Fuchs, Geofis. Pura Appl. **51** (1963) 185.
[96] J. Bricard, Geofisica pura e applicata **51** (1962) 237.
[97] W. H. Marlow, The Journal of Chemical Physics **73** (1980) 6284.
[98] A. A. Lushnikov, and M. Kulmala, Physical Review E **70** (2004) 046413.
[99] W. A. Hoppel, and G. M. Frick, Aerosol Science and Technology **5** (1986) 1.
[100] L. G. D'Yachkov, A. G. Khrapak, S. A. Khrapak, and G. Morfill, Physics of Plasmas **14** (2007)
[101] X. Lopez-Yglesias, and R. C. Flagan, Aerosol Science and Technology **47** (2013) 688.
[102] M. Lampe, and G. Joyce, Physics of Plasmas **22** (2015) 023704.
[103] F. Taccogna, S. Longo, and M. Capitelli, Eur. Phys. J. AP **22** (2003) 29.
[104] D. Trunec, M. Holík, P. Kudrna, O. Bilyk, A. Marek, R. Hippler, and M. Tichý, Contrib. Plasma Phys. **44** (2004) 577.
[105] F. Iza, and J. K. Lee, Journal of Vacuum Science & Technology A: Vacuum, Surfaces, and Films **24** (2006) 1366.
[106] S. A. Khrapak, A. P. Nefedov, O. F. Petrov, and O. S. Vaulina, Physical Review E **59** (1999) 6017.
[107] S. A. Khrapak, G. E. Morfill, A. G. Khrapak, and L. G. D'Yachkov, Physics of Plasmas **13**, 052114 (2006)
[108] S. A. Khrapak, A. V. Ivlev, G. E. Morfill, H. M. Thomas, S. K. Zhdanov, U. Konopka, M. H. Thoma, and R. A. Quinn, Physics of Plasmas **10** (2003) 4579.
[109] C. Zafiu, A. Melzer, and A. Piel, Physics of Plasmas **10** (2003) 4582.
[110] M. A. Fink, M. H. Thoma, and G. E. Morfill, Microgravity Science and Technology **23** (2011) 169.
[111] M. H. Thoma, M. A. Fink, H. Hofner, M. Kretschmer, S. A. Khrapak, S. V. Ratynskaia, V. V. Yaroshenko, G. E. Morfill, O. F. Petrov, A. D. Usachev, A. V. Zobnin *et al.*, Ieee Transactions on Plasma Science **35** (2007) 255.

[112] M. H. Thoma, H. Hofner, M. Kretschmer, S. Ratynskaia, G. E. Morfill, A. Usachev, A. Zobnin, O. Petrov, and V. Fortov, Microgravity Science and Technology **18** (2006) 47.
[113] M. H. Thoma, S. A. Khrapak, R. A. Quinn, G. E. Morfill, O. Petrov, and V. Fortov, Ukrayins'kij Fyizichnij Zhurnal (Kiev) **50** (2005) 179.
[114] V. Fortov, G. Morfill, O. Petrov, M. Thoma, A. Usachev, H. Hoefner, A. Zobnin, M. Kretschmer, S. Ratynskaia, M. Fink, K. Tarantik *et al.*, Plasma Physics and Controlled Fusion **47** (2005) B537.
[115] A. Usachev, A. Zobnin, O. Petrov, V. Fortov, M. Thoma, M. Kretschmer, S. Ratynskaia, R. Quinn, H. Hoefner, and G. Morfill, Czechoslovak Journal of Physics **54** (2004) C639.
[116] S. Ratynskaia, S. Khrapak, A. Zobnin, M. H. Thoma, M. Kretschmer, A. Usachev, V. Yaroshenko, R. A. Quinn, G. E. Morfill, O. Petrov, and V. Fortov, Physical Review Letters **93** (2004) 085001.
[117] S. A. Khrapak, S. V. Ratynskaia, A. V. Zobnin, A. D. Usachev, V. V. Yaroshenko, M. H. Thoma, M. Kretschmer, H. Höfner, G. E. Morfill, O. F. Petrov, and V. E. Fortov, Physical Review E **72** (2005) 016406.
[118] S. A. Khrapak, P. Tolias, S. Ratynskaia, M. Chaudhuri, A. Zobnin, A. Usachev, C. Rau, M. H. Thoma, O. F. Petrov, V. E. Fortov, and G. E. Morfill, EPL (Europhysics Letters) **97** (2012) 35001.
[119] S. Chandrasekhar, Reviews of Modern Physics **15** (1943) 1.
[120] I. Snook, *The Langevin and Generalised Langevin Approach to the Dynamics of Atomic, Polymeric and Colloidal Systems* (Elsevier Science, 2006),
[121] P. Langevin, Ann. Chim. Phys. **28** (1903) 289.
[122] W. T. Coffey, Y. P. Kalmykov, and J. T. Waldron, *The Langevin Equation* (WORLD SCIENTIFIC, 2004), Vol. Volume 14, World Scientific Series in Contemporary Chemical Physics, Volume 14
[123] H. Risken, and T. Frank, *The Fokker-Planck Equation: Methods of Solution and Applications* (Springer Berlin Heidelberg, 1996),
[124] Z. Schuss, *Brownian Dynamics at Boundaries and Interfaces: In Physics, Chemistry, and Biology* (Springer New York, 2013),
[125] L. Li, and R. Gopalakrishnan, Journal of Aerosol Science **151** (2021) 105678.
[126] L. Li, H. S. Chahl, and R. Gopalakrishnan, Journal of Aerosol Science **140** (2020) 105481.
[127] R. Gopalakrishnan, P. H. McMurry, and C. J. Hogan, Aerosol Science and Technology **49** (2015) 1181.
[128] R. Gopalakrishnan, T. Thajudeen, H. Ouyang, and C. J. Hogan, Journal of Aerosol Science **64** (2013) 60.
[129] R. Gopalakrishnan, M. J. Meredith, C. Larriba-Andaluz, and C. J. Hogan, Journal of Aerosol Science **63** (2013) 126.
[130] D. L. Ermak, and H. Buckholz, Journal of Computational Physics **35** (1980) 169.
[131] C. N. Davies, Proceedings of the Physical Society **57** (1945) 259.
[132] E. Cunningham, Proceedings of the Royal Society of London. Series A. **83** (1910) 357.
[133] B. Liu, J. Goree, V. Nosenko, and L. Boufendi, Physics of Plasmas **10** (2002) 9.
[134] P. S. Epstein, Physical Review **23** (1924) 710.
[135] S. D. Baalrud, and J. Daligault, Physics of Plasmas **26** (2019) 082106.
[136] P. Mazur, and I. Oppenheim, Physica **50** (1970) 241.
[137] V. Suresh, L. Li, J. R. G. Felipe, and R. Gopalakrishnan, Journal of Physics D: Applied Physics **54** (2021) 275205.
[138] J. Albers, J. M. Deutch, and I. Oppenheim, The Journal of Chemical Physics **54** (1971) 3541.
[139] V. Suresh, and R. Gopalakrishnan, Journal of Aerosol Science **155** (2021) 105746.
[140] S. Dutta, and S. A. Rangwala, Physical Review A **97** (2018) 041401.
[141] B. M. Smirnov, Phys. Scr. **61** (2000) 595.
[142] A. V. Phelps, H. G. Chris, J. J. P. Burke, and A. V. Phelps, Journal of Physics B: Atomic, Molecular and Optical Physics **33** (2000) 2965.
[143] U. R. Kortshagen, R. M. Sankaran, R. N. Pereira, S. L. Girshick, J. J. Wu, and E. S. Aydil, Chemical Reviews **116** (2016) 11061.
[144] M. Davide, and R. M. Sankaran, Journal of Physics D: Applied Physics **43** (2010) 323001.

[145] T. Lafleur, J. Schulze, and Z. Donkó, Plasma Sources Science and Technology **28** (2019) 040201.
[146] V. E. Fortov, O. F. Petrov, A. D. Usachev, and A. V. Zobnin, Physical Review E **70** (2004) 046415.

Predictor-Corrector iteration

Predictor step: Ion scale

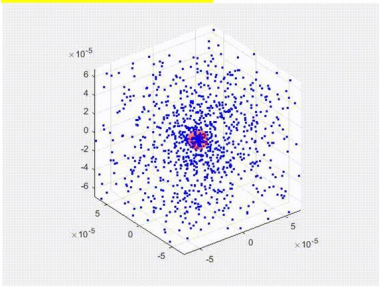

$N_t \sim 60 - 700$ particle-ion collisions

Iterate until convergence of
- **Grain charge**
- **Ion Drag force**
- **Grain drift velocities**

$M_t \sim 10000$ timesteps

Corrector step: Particle scale

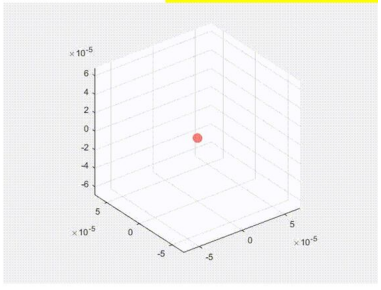

Steady state: $\vec{F}_{id} - f_p \langle \vec{v}_p \rangle_{drift} + z_p e \vec{E}_0 = 0$